Optimizing sulfur emission control areas for shipping

Lu Zhen[1], Dan Zhuge[1], Shuanglu Zhang[1], Shuaian Wang[2*], Harilaos N. Psaraftis[3]

[1]*School of Management, Shanghai University, Shanghai, China*
[2]*Department of Logistics and Maritime Studies, The Hong Kong Polytechnic University, Kowloon, Hong Kong*
[3] *Department of Technology, Management and Economics, Technical University of Denmark, 2800 Kgs Lyngby, Denmark*
* Corresponding author: hans.wang@polyu.edu.hk

Abstract: The design of emission control areas (ECAs), including ECA width and sulfur limits, plays a central role in reducing sulfur emissions from shipping. To promote sustainable shipping, we investigate an ECA design problem that considers the response of liner shipping companies to ECA designs. We propose a mathematical programming model from the regulator's perspective to optimize the ECA width and sulfur limit with the aim of minimizing the total sulfur emissions. Embedded within this regulator's model, we develop an internal model from the shipping liner's perspective to determine the detoured voyage, sailing speed, and cargo transport volume with the aim of maximizing the liner's profit. Then, we develop a tailored hybrid algorithm to solve the proposed models based on the variable neighborhood search meta-heuristic and a proposition. We validate the effectiveness of the proposed methodology through extensive numerical experiments and conduct sensitivity analyses to investigate the effect of important ECA design parameters on the final performance. The proposed methodology is then extended to incorporate heterogeneous settings for sulfur limits, which can help regulators to improve ECA design in the future.

Keywords: Sustainable shipping; emission control area (ECA) design; cargo allocation; path and speed optimization; sulfur emissions

1. Introduction

Maritime shipping plays an important role in global trade and supply chain operations (Fransoo & Lee, 2013; Meng et al, 2014; Tierney et al., 2015; Roy et al., 2020). However, maritime transportation imposes a severe pollution burden on the global environment and adversely affects sustainable development because ships burn bunker fuel with a much higher sulfur content than other modes of transportation when comparing emissions by weight or volume of cargo. Maritime shipping activities account for about 12% of the global anthropogenic sulfur oxides (SO_x) emissions (Wang et al., 2021). The extensive SO_x emissions cause serious harm to both the environment and people's health, with undesirable consequences such as acid rain, lung cancer, cardiovascular disease, and some birth defects being related to anthropogenic SO_x emissions (Dai et al., 2019). Therefore, the International Maritime Organization (IMO) and regional regulators around the world have established emission control areas (ECAs) to reduce damage to the environment and human health caused by sulfur emissions from

shipping. ECAs have specified limits that are lower than most ocean areas for the content of SO_x in ships' exhausts. Outside ECAs, the global sulfur cap, which became effective from January 1, 2020, imposes a sulfur content limit for fuel of 0.5% (previously it was 3.5%). Figure 1 shows some of the ECAs around the world, including an ECA in China. The IMO recently decided to designate the Mediterranean Sea an ECA with a sulfur cap of 0.1%, which will become effective from May 1, 2025 (UNEP, 2022). The established and planned ECAs raise the question of whether the regulation of ECAs is reasonable and helpful in emissions abatement efforts. Therefore, further discussion and analysis is required of the effectiveness of different ECA regulations in terms of ECA boundaries and the fuel sulfur content limits within ECAs, and the effects on total sulfur emissions to provide a reference for regulatory decision-making.

Figure 1: Existing ECAs around the world and China's ECA

Figure 1 indicates that the features of ECAs established in different areas are not identical. Regulators (i.e., countries' governments or the IMO) may design ECAs differently and impose different sulfur limits depending on the shapes of the ECAs' territories and the distance between the ECA's boundary and the coastline. For example, ships sailing in China's ECA are required to use fuel with a sulfur content not exceeding 0.5%, a limit that was set when the global sulfur cap was 3.5%. Recently, China's regulator has considered lowering the sulfur cap to 0.1%. The ECA in China differs from those in some European and American sea areas; in contrast to Europe and North America for instance, where ECA boundaries either are not linked to a specific distance from the coastline or can go up to 200 nautical miles (nm) from it, the boundary of China's ECA is only 12 nm from the coastline. Sulfur limits and the ECA boundary's distance from the coastline are two crucial decision variables for ECA design, and they significantly influence the extent to which sulfur emissions are reduced by the ECA. In reality, the decisions on a country's ECA design are mainly made according to the current level of green technology implemented in a country's ships, the experts' experience and predictions on the development of green shipping technology, the regulator's long-term targets (or commitments) concerning environmental protection, and other political factors. For example, China's ECA boundary was set at 12 nm simply

because this is the breadth of China's territorial seas, whereas in other countries, the ECA boundary and the territorial sea boundary are not necessarily identical. The ECA boundary and the sulfur limit should be decided in a more rigorous, scientific, and optimization-based manner than the current system to minimize society's total sulfur emissions, which should be the ultimate purpose of establishing ECAs.

With the aim of minimizing total sulfur emissions for society, the optimal design of an ECA should neither be laid out with as large an area as possible, nor impose as strict a sulfur content limit as possible. The reason for this is that the establishment of an ECA may compel ships that are not equipped with scrubbers (which reduce the sulfur content in a ship's exhaust) to make detours that increase the length of their voyage outside the ECA, where they use cheaper high-sulfur fuel rather than the more expensive low-sulfur fuel they use inside the ECA (Fagerholt et al., 2015; Fagerholt & Psaraftis, 2015; Zhen et al., 2018; Li et al., 2020; Wang et al., 2021). For understanding the detour behavior under the context of the ECA, an example is shown in Figure 2.

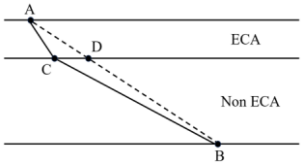

Figure 2: Illustration of the detour behavior under the context of the ECA

We analyze the detour behavior for sailing from Port A to Port B by comparing two sailing paths, i.e., a path from A to B directly via point D on the ECA boundary, and a path from A to B via detour point C on the ECA boundary. We can see in Figure 2 that the distance AC is shorter than the distance AD, and thus sailing along AC can reduce the consumption of the high-price marine fuel used within the ECA; we can also see that the distance BC is longer than the distance BD, so sailing along BC consumes more low-price fuel used outside the ECA. When the cost of the reduced high-price fuel consumption via sailing along AC (instead of AD) is higher than the cost of the increased low-price fuel consumption via sailing along BC (instead of BD), sailing along the path from A to B via detour point C can reduce the fuel cost. Therefore, the detour behavior (i.e., sailing from A to B via detour point C) may be conducted for reducing the fuel cost.

The initial purpose of setting up the ECA is to reduce air pollution near the shore. From a theoretical perspective, a government should set as large ECA territory and as strict ECA policy as possible for minimizing the ships' emission near the shore. The larger the ECA territory or the stricter its sulfur limit, the longer the detours and sea transportation time between ports. In addition, the stricter its sulfur limit, the more expensive marine fuel should be consumed inside the ECA; then the sea transportation cost increases. As a consequence, long sea transportation times and high sea transportation cost may lead to

some cargoes being transported by land instead of sea, and thus the policy may have the paradoxical effect of increasing sulfur emissions because sulfur emissions per unit weight of cargo are much higher for land transportation than for sea transportation. In this case, implementing a stricter "green" environmental policy may have the unintended effect of actually worsening environmental outcomes. Therefore, we conduct an explorative study on how to optimize the ECA design using mathematical model-based methods to minimize the total sulfur emissions for society.

As the regulator is the decision-maker for the ECA design, this study first formulates a mathematical programming model with the ECA boundary and the sulfur limit as the decision variables, and the objective of minimizing the total sulfur emissions used in fulfilling the cargo transportation demands among a network of ports (or cities) via both sea and land routes. In the regulator's model, there are some parameters that are decisions, directly or indirectly, for shipping liners, such as the detoured voyages in the shipping network, ship speeds inside and outside the ECAs, and transportation volumes via sea and land routes. Thus, as well as the regulator's model, we formulate a liner's model designed to maximize the liner's profit, with the above mentioned "parameters" as decision variables. The liner's model can be regarded as an "inner model" embedded within the regulator's model. We also propose algorithms to solve these models efficiently. Using data on the transportation demand within the network of the major ports (cities) along China's coastline, we apply our proposed methodology (i.e., our models and algorithms) to the design of an ECA for China's offshore sea. The optimal ECA design that we obtain suggests that the current ECA boundary, which is 12 nm from the coastline, could be moved inward, closer to the coastline, to 11 nm. In addition, we obtain an optimal sulfur limit of 0.1%, which is stricter than the current 0.5% limit in China. These results could assist regulators to reconsider ECA designs. Moreover, in a novel extension, we broaden the proposed methodology to a generic context by considering an ECA that is heterogeneous with respect to sulfur limits. Although most current ECAs are homogenous, our extended methodology could be applied to develop a cutting-edge heterogeneous ECA design, which could further help regulators to improve ECA designs in the future. The experimental results in this study indicate that the solved optimal heterogeneous ECA design can reduce sulfur emissions by an additional 5% above those achieved under the homogeneous ECA design with the lowest emissions limit. Moreover, the proposed methodologies in this study are potentially useful for designing environmentally friendly policies in other fields.

The remainder of this paper is organized as follows. The related literature is reviewed in the next section. Section 3 describes the problem background in detail. The mathematical models for the regulator and the shipping liners are formulated in Section 4. Then, algorithms for solving the models efficiently are suggested in Section 5. Numerical experiments based on the real data and the background

of China's offshore sea ECA are conducted in Section 6, in which we derive some managerial insights for both the regulator and the liners. Section 7 and Section 8 further extends the methodology to more complex contexts. Finally, we outline our conclusions in the last section.

2. Literature review

This study belongs to the field of maritime transportation, which has received considerable attention in the scientific literature (Agarwal & Ergun, 2010; Choi et al., 2012; Li et al., 2015; Lu et al., 2017; Wang & Meng, 2020; Lee et al., 2021). Specifically, our research relates to the effects of ECAs on shipping operations, shipping emission reductions, the modal shift from sea to land transport, and, in particular, the design of ECAs for ships.

The optimization of shipping operations under ECAs has been the focus of intensive research in recent years (Doudnikoff & Lacoste, 2014; Gu & Wallace, 2017; Cariou et al., 2018; Ma et al., 2021; Tan et al. 2022). Fagerholt et al. (2015) investigated the sailing speeds and paths for a ship sailing in a given sequence between several ports and found that ships would often sail a longer total distance than would otherwise be required to reduce the distance that they traveled within ECAs, and that they would sail at different speeds within and outside ECAs. Fagerholt and Psaraftis (2015) demonstrated that sailing speeds are lower within ECAs than outside them and explored the factors influencing this speed difference. Zhen et al. (2018) identified that ships can reduce their fuel cost by making detours and sailing at a lower speed within ECAs. Zhen et al. (2020) designed a model of sailing speeds and routes in areas with different sulfur limits with the aim of simultaneously minimizing the total fuel cost and SO_x emissions. They also conducted sensitivity analyses on ECA boundaries, decision-makers, and fuel costs. Li et al. (2020) optimized the detour strategy and sailing pattern after the implementation of ECA regulations. Wang et al. (2021) addressed a joint shipping network optimization problem on sailing speed and path design, schedule design, and fleet deployment under ECAs. Their numerical experiments showed that detour strategies and lower speeds within ECAs can contribute to cost savings.

Many studies have analyzed the effect of ECAs on shipping emissions. Browning et al. (2012) concluded that switching to marine gas oil (MGO) in ECAs can significantly reduce SO_x and particulate matter (PM) emissions, and slightly reduce nitrogen oxides (NO_x) emissions. Chang et al. (2014) measured the SO_x, NO_x, and PM emissions from ships in a potential ECA at Seoul's Port of Incheon and confirmed that the 0.1% sulfur limit can reduce these emissions by up to 93%. Chen et al. (2018) identified that a potential ECA in the Mediterranean Sea would cause detour behavior and emission reduction. Svindland (2018) analyzed the sulfur emissions of a shipping service and an alternative road haulage operation before and after the implementation of ECA regulations. Sheng et al. (2019) and Ma

et al. (2020) found that ECA regulations would reduce local SO_x emissions but increase global CO_2 emissions. Zhang et al. (2020) adopted the regression discontinuity approach to analyze the effect of an ECA in Shanghai, and demonstrated that the ECA regulation was effective in reducing SO_x emissions.

Modal shifts caused by the ECA regulations have been a key topic in many studies. Holmgren et al. (2014) discussed the possibility of a modal shift from sea to land transport between Lithuania and the United Kingdom, but found that for relatively high-value cargoes, a shift to land transport was nearly impossible. Panagakos et al. (2014) compared a road-only option and a combined-transport option incorporating both road and sea transport. They predicted that designating the Mediterranean Sea as an ECA would cause a modal shift to the road-only option. Vierth et al. (2015) observed that increasing the strictness of sulfur limits may lead to a modal shift from sea to road and rail. Zis & Psaraftis (2017) examined how to shut down some shipping routes and redistribute cargo flows to land transport under ECA regulations, and further recommended how to reverse these negative side-effects. Zis et al. (2019) and Zis & Psaraftis (2019) provided measures to mitigate possible modal shifts under sulfur limit regulations. Zisi et al. (2021) conducted an analysis to examine the impact of the 2020 sulfur cap on CO_2 emissions.

The negative effects of ECAs are not always anticipated and thus improving the effectiveness of ECAs is crucial. Sun et al. (2020) determined fictitious sulfur emission permits for shipping carriers and optimized the location of ECAs to minimize the impact of sulfur emissions on human health. Li et al. (2022) determined an extreme ECA boundary to reduce the expected shipping emissions considering the effect of the ECA boundary on ships' detour strategies.

Overall, there has been limited research on ECA design optimization. To narrow the research gap in the ECA design field, this study proposes a model from the regulator's perspective to optimize ECA width (i.e., the ECA boundary's distance to the coastline) and sulfur limits with the aim of minimizing the total sulfur emissions via sea and land transport. Combined with, or embedded in, this regulator's decision model, we propose a model from the liners' perspective to determine the detoured voyages, sailing speed, and cargo transport volume via sea and land routes with the aim of maximizing profit.

3. Problem description

Although ECAs in the world have different shapes from the perspective of topology, this paper firstly conducts an analytical study for the most basic topology of the ECA, in which the ECA boundary's distance to the coastline is a constant value; here the distance is called as "ECA width" in this study. For understanding the topology of the ECA, the region marked with green color in the right-bottom part of Figure 3 denotes the ECA along the coastline. It should be noted that the ECA along the coastline

may have the different ECA widths along the different segments of the coastline in some realistic contexts. However, this study oriented to the constant ECA width can act as the basis to derive analytical results for the ECAs with more complex topological considerations.

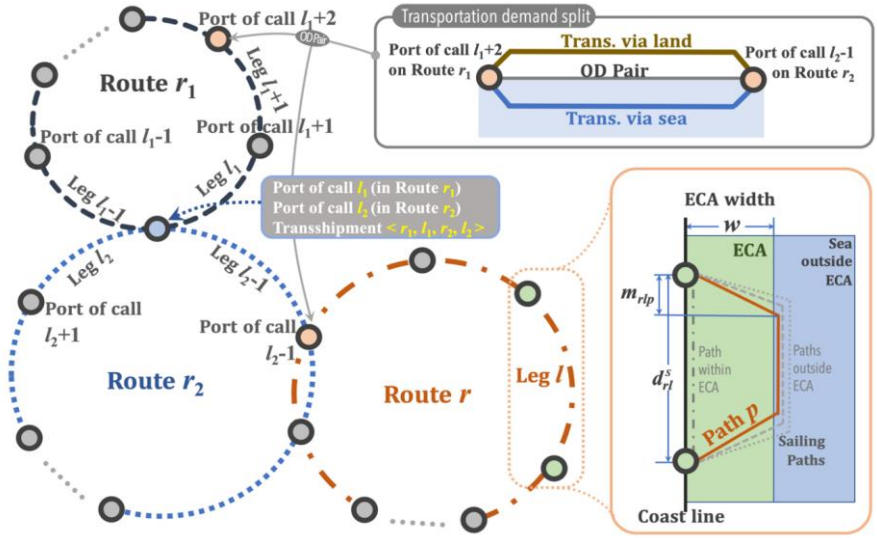

Figure 3: A shipping network with three routes in the context of an ECA

Suppose that a regulator establishes an ECA and has to determine two variables: the ECA width and the sulfur content limit. The former is the distance between the coastline and the ECA boundary, denoted by w; the latter specifies that the sulfur content of ship fuel consumed within the ECA should not exceed a limit, denoted by x, and the set of all the possible limits is denoted by X. The ECA has a significant influence on a shipping liner's operations, which are carried out within a shipping network with a set I of seaports, indexed by i or j. As shown in Figure 3, the three circular paths denote three shipping routes; the small circles located on the above three large circular paths denote different seaports (or ports of call in routes). Suppose that there are a set R of shipping routes indexed by r. Each route r contains a set L_r of ports of call (or legs) indexed by l; here, leg l is from port of call l to port of call $l+1$, as shown in Figure 3.

Suppose the target of the regulator is to minimize the total sulfur emissions in the process of fulfilling all the transportation demands among a given set Y of origin–destination (OD) pairs, which are indexed by (i,j). In this study, all the OD pairs' cities are along the coastline; and the two directions of the transportation flow for each OD pair are considered. The volume of cargo (measured in 20-foot equivalent unit containers, known as TEUs) that needs to be transported for each OD pair (i,j) is

denoted by parameter q_{ij}. We assume that the transportation demand in each OD pair can be fulfilled by either maritime shipping via sea, or road transportation via land, as shown in the top-right part of Figure 3. The design of the ECA, including width w and limit x, may affect an OD's delivery time via sea (denoted by a decision variable θ_{ij}^{S} for OD pair (i,j)), which may further influence the consigners in choosing sea or land transportation for their cargoes. More specifically, for each OD pair (i,j), the parameter q_{ij} on cargo volume is split into two decision variables α_{ij}^{S} and α_{ij}^{L}, which denote the volume (TEU) transported for the OD pair (i,j) via sea and land, respectively. The abovementioned delivery duration θ_{ij}^{S} for OD pair (i,j) via sea is a variable, whereas the delivery duration for the OD pair via land is a parameter denoted by t_{ij}^{L} because our focus is on the ECA design, which has little influence on the land transportation time. In the demand split, the carrier of land transportation in this study could be regarded as a dummy group of the logistics companies who undertake the land transportation tasks of the OD pairs in the shipping network. Because this study focuses on the ECA design in the sea, the details of the land transportation are simplified; we do not distinguish the logistics companies in the land transportation with respect to their unit transportation cost, unit emissions and so on. In a maritime context, demand split depends on the particular context. In a deep sea (intercontinental) context, e.g., from Far East to Europe, rail is the main land alternative to shipping, and in fact rail services exist and their use versus the maritime mode depends on many factors (Psaraftis and Kontovas, 2010; Qi et al., 2022). In a short sea context for instance in Europe, road (truck) is the typical alternative (Zis & Psaraftis, 2017 and 2019) in the context of the analysis of impacts of sulfur regulations in Northern Europe.

In fact demand split among multiple transportation methods is generally a highly complex issue for both academia and practitioners, as many explicit and implicit factors influence the demand split. Because the core decision that we investigate (the design of the ECA) mainly affects the sea voyage time (Zhen et al., 2020; Wang et al., 2021), we assume that the demand split between the sea and land methods is based on their relative delivery times. The demand split according to the delivery/travel time has also been studied in literature. For example, Chou et al. (2010) investigate container transportation demand split and find that shippers are not only concerned by the inland freight cost but also the frequency of ship callings at ports, which implies the delivery time is an important metric in the transportation demand split. Xiong et al. (2020) also investigate the demand split in the context of pickup and delivery, and indicate that demands can be split and transported mainly according to the length of the paths, which is actually equivalent to the paths' travel time. For the passenger travel demand split, Li & Shang (2016) also conclude that route travel time is the most important factor affecting the market share of the air transport and high-speed railway services. In a maritime context,

demand split is considered by (among others), Psaraftis & Kontovas (2010) and Qi et al. (2022) for deep sea (intercontinental) shipping, and by Zis & Psaraftis (2017 and 2019) for short sea shipping. Thus, this study considers the demand split in our model, and the split is mainly based on the delivery time of the cargoes along different ways. In addition, it should be noted that shippers do not choose either land or sea for the entire O-D demand; while this study considers the demand split in percentages between the land and the sea ways, e.g., 40% sea, 60% land for an OD pair; these percentages are decision variables in our model, and is dependent on the aforementioned delivery time of the cargoes along different ways. More specifically, for each OD pair (i, j), we have the demand $q_{ij} = \alpha_{ij}^{L} + \alpha_{ij}^{S}$, and we assume that $\alpha_{ij}^{L}/\alpha_{ij}^{S} = \theta_{ij}^{S}/t_{ij}^{L}$. The demand split can be extended to consider more complex factors using the same methodology in future studies.

The influence of the ECA's design on voyage time is reflected in the selection of paths among the multiple sailing paths for each leg. For each leg l on route r, the set of sailing paths is denoted by P_{rl}, and each path is indexed by p. It is noted that a path within the ECA is also included in the set P_{rl}; the path is a route that is close to the coastline between the two ports of the leg l on route r. The selection among the multiple paths is defined as a binary decision variable λ_{rlp} that equals one if ships sail on path $p \in P_{rl}$ of route r's leg l. Studies have shown that the most cost-saving path is not always the shortest path when an ECA exists (Zhen et al., 2018; Li et al., 2020; Wang et al., 2021); as we noted earlier, this results in the phenomenon of voyage detours under ECAs. The optimal path is influenced by the ECA width, and the ratio of the unit cost of fuel consumed inside the ECA to the unit cost of fuel consumed outside the ECA (Zhen et al., 2020; Wang et al., 2021; Li et al., 2022). As shown in Figure 3, a parameter m_{rlp} is defined to reflect the degree of the detour for path $p \in P_{rl}$ of leg l on route r under the ECA; d_{rl}^{S} is defined as the coastline distance of leg $l \in L_r$ on route r. Based on the above definition, we can derive that the sailing distances inside and outside the ECA for path $p \in P_{rl}$ of leg l on route r are $2(w^2 + m_{rlp}^2)^{1/2}$ and $d_{rl}^{S} - 2m_{rlp}$, respectively.

Moreover, the sailing speeds within and outside the ECA on path p are denoted by v_{rlp}^{E} and v_{rlp}^{N}, respectively. These speeds influence the voyage time, may affect the transportation volume via sea, and ultimately affect the shipping liner's revenue. In addition, the speeds determine the unit fuel consumption, which influences the liner's costs. In this study, the function for calculating ships' fuel consumption per unit of distance on the basis of the ships' sailing speed follows the widely used formula of $a \cdot speed^{b}$ (ton/nm), where a and b are parameters in the fuel function (Wang & Meng, 2012). Furthermore, the sulfur emissions from consuming a ton of marine fuel inside and outside the ECA are denoted by $s^{E}(x)$ and s^{N}, respectively. As the sulfur content of ship fuel consumed within the ECA

should not exceed the limit x, the unit emission $s^E(x)$ is related to x. When ships are outside the ECA, we assume that they will use the cheapest fuel available; thus, the unit emission s^N is a constant. Based on the above definition, we can derive that the sulfur emissions inside and outside the ECA for path $p \in P_{rl}$ of leg l on route r are $s^E(x)a\left(v_{rlp}^E\right)^b 2(w^2 + m_{rlp}^2)^{1/2}$ and $s^N a\left(v_{rlp}^N\right)^b \left(d_{rl}^S - 2m_{rlp}\right)$, respectively. Land transportation also generates sulfur emissions. Suppose that s^D is the sulfur emissions per ton of diesel fuel consumed by trucks, and u_{ij}^L is the diesel fuel consumption per TEU for OD pair (i,j) via land (ton/TEU). Recall that α_{ij}^L is defined as the volume (TEU) of cargoes transported via land. Then, we can derive that the total sulfur emissions via land are $\sum_{(i,j)\in Y} s^D u_{ij}^L \alpha_{ij}^L$. By summarizing the above, the objective for the regulator's decision model should be formulated as $\sum_{r\in R} n_r \sum_{l\in L_r} \sum_{p\in P_{rl}} \lambda_{rlp}^* \left[s^E(x)a\left(v_{rlp}^{E*}\right)^b \left(2\sqrt{w^2 + m_{rlp}^2}\right) + s^N a\left(v_{rlp}^{N*}\right)^b \left(d_{rl}^S - 2m_{rlp}\right)\right] + \sum_{(i,j)\in Y} s^D u_{ij}^L \alpha_{ij}^{L*}$, which represents the total sulfur emissions in the process of fulfilling all the transportation demands among a given set of OD pairs, and the regulator should minimize it by determining an appropriate ECA width w as well as an appropriate sulfur content limit x.

Some notations that are indicated by a superscript asterisk are parameters in the regulator's decision model, but they should be decided within the shipping liner's decision model, the objective of which is to maximize the shipping liner's profit by transporting more containers via sea and reducing its operational costs, such as fuel. The shipping liner's decisions occur within the ECA context, which means that the ECA width w and the sulfur content limit x are parameters in the shipping liner's model. Therefore, as well as a regulator model, we formulate a liner's model, and the two models are intertwined, with common variables and parameters. The liner's model is essentially an indispensable component embedded in the regulator's model.

As noted, the aim of this study is to investigate the design of an ECA within the context of the shipping network. Therefore, the cargo transshipment in the network ports should be considered, as Figure 3 shows. In reality, there may be no direct ship route for an OD pair. Therefore, the cost of transshipping containers should be incorporated into the liner's model as well as the fuel cost. Moreover, the calculation of the delivery time for an OD pair should consider the transshipped containers' dwell time at transshipment ports. The dwell time is calculated as the difference between the two routes' arrival times at the transshipment port, which is part of the timetable design issue for the liner. Thus, the issues related to timetables are decision variables in the liner's model as well as being considered in the regulator's model. The details of the models are elaborated in the next section.

Before formulating the decision models for the regulator and the shipping liner, we summarize the

assumptions adopted in this study as follows.

(1) The ECA is homogenous with respect to the width and the sulfur content limit.

(2) Two transportation methods via sea and land are considered in the demand split for each OD pair. The split is based on ratio of the delivery times of the two methods and ignores more complex relationships and factors such as freight cost.

(3) The capacity for sea transportation is sufficient. Emissions from sea transport are mainly related to the network constituted by linked voyage paths; they are not proportional to the number of transported TEU containers because a ship's unit emissions mainly depend on its speed rather than the weight of the cargo carried. Conversely, the emissions from land transportation are proportional to the number of transported TEUs because containers are carried by individual trucks.

Finally, we highlight some additional remarks. First, we do not consider ships equipped with scrubbers, which can reduce the sulfur content in ships' exhausts, such that the ships do not need to detour to reduce the distance traveled within the ECA. Moreover, for the demand split, we do not consider the full transportation demand of each OD pair, but only the component of demand that is sensitive to a change in the delivery time in response to the ECA. Thus, we exclude consideration of demand for cargo transport that is not sensitive to the delivery time when the cargo owners decide whether to use land or sea transport. Therefore, the objective value considered by the regulator's model is the total sulfur emissions from the transportation activities of ships without scrubbers for fulfilling the demand of the OD pairs in the network as defined above, rather than being the sulfur emissions for all the transportation activities in the network.

4. Mathematical models

This section proposes two mathematical models. The first model's decision-maker is the regulator, who aims to minimize total emissions by designing the ECA with an appropriate sulfur limit and width. The second model's decision-maker is the shipping liner, who aims to maximize profit by adjusting their operational-level decisions (e.g., sailing paths, speeds, and cargo allocation in the shipping network) under the ECA policy decided by the regulator. The decisions by the two parties (i.e., regulator and liner) are intertwined and influence each other. Although the core decisions investigated in this study are contained in the first model, the second model is also important and necessary. This section elaborates on the formulations of the two models.

4.1 Notations for parameters and variables

Before formulating the two models, the notations for the parameters and decision variables are listed as follows. For easy understanding, the parameters and the variables are denoted by the Roman letters

and the Greek letters, respectively.

Sets and indices

R	set of routes, indexed by r.
L_r	set of ports of call (or legs) on route r, indexed by l, leg l is from port of call l to $l+1$.
P_{rl}	set of sailing paths for leg $l \in L_r$ of route r, indexed by p.
I	set of ports, indexed by i or j.
i_{rl}	index of the port that corresponds to the l^{th} port of call on ship route r, $i_{rl} \in I$.
Y	set of OD pairs, indexed by (i,j), $Y = \{(i,j) \mid i \in I, j \in I\}$.
$\langle r_1, l_1, r_2, l_2 \rangle$	a transshipment from the l_1^{th} port of call on route r_1 to the l_2^{th} port of call on route r_2; $r_1, r_2 \in R$; $l_1 \in L_{r_1}$, $l_2 \in L_{r_2}$. The quadruple $\langle r_1, l_1, r_2, l_2 \rangle$ implies the two ports of call on the two routes correspond to the same physical port in the shipping network, i.e., $i_{r_1,l_1} = i_{r_2,l_2}$.
U	set of quadruples $\langle r_1, l_1, r_2, l_2 \rangle$; $U = \{\langle r_1, l_1, r_2, l_2 \rangle \mid i_{r_1,l_1} = i_{r_2,l_2}\}$.
X	set of alternatives of sulfur content limit of fuel consumed within ECA, indexed by x.

Parameters

w	ECA width (i.e., the distance between coastline and ECA boundary). It is a variable in the first model and a parameter in the second model.
g	length of period (in days) for vessels' periodical visits at ports in the shipping network.
q_{ij}	total volume (TEU) of cargoes that need be transported for OD pair (i,j) via sea or land.
$s^E(x)$	sulfur emission of consuming per ton of marine fuel with x sulfur content.
s^N	sulfur emission of consuming per ton of marine fuel consumed outside the ECA.
s^D	sulfur emission of consuming per ton of diesel fuel for trucks.
a, b	parameters for calculating the ship's fuel consumption per unit distance on the basis of the ship's sailing speed, i.e., $a \cdot speed^b$ (ton/n mile).
u_{ij}^L	diesel fuel consumption per TEU for OD pair (i,j) via land (ton/TEU).
c_{ij}^S	unit price (USD/TEU) of shipping containers for OD pair (i,j) via sea.
c_{r_1,l_1,r_2,l_2}^H	unit handling cost (USD/TEU) for transshipping containers at the port $\langle r_1, l_1, r_2, l_2 \rangle$.
$f^E(x)$	unit cost of marine fuel with x sulfur content (USD/ton).
f^N	unit cost of marine fuel consumed outside the ECA (USD/ton).
$\overline{v}$	maximum sailing speed (knot) of ships.
d_{rl}^S	coastline distance of leg $l \in L_r$ on route r.

m_{rlp} distance that reflects the detour degree for path $p \in P_{rl}$ of leg l on route r under the ECA.

e_{rl} ship's dwell duration (hours) at the l^{th} port of call on route r.

$k^H_{r_1,l_1,r_2,l_2,i,j}$ equals one if the transshipment $\langle r_1, l_1, r_2, l_2\rangle$ is used for OD pair (i,j), and zero otherwise.

k^S_{rlij} equals one if the leg l on route r is used for OD pair (i,j), and zero otherwise.

t^L_{ij} delivery duration for OD pair (i,j) via land.

y_r number of ships deployed on route $r \in R$.

Decision variables

λ_{rlp} binary, equals one if ships sail on path $p \in P_{rl}$ of leg l on route r, and zero otherwise.

α^S_{ij} volume (TEU) of cargoes transported for OD pair (i,j) via sea.

α^L_{ij} volume (TEU) of cargoes transported for OD pair (i,j) via land.

v^E_{rlp} sailing speed within the ECA on path $p \in P_{rl}$ of leg l on route r.

v^N_{rlp} sailing speed outside the ECA on path $p \in P_{rl}$ of leg l on route r.

τ_{rl} sailing time (hours) on leg $l \in L_r$ of route r.

θ^S_{ij} delivery duration for OD pair (i,j) via sea.

π_{rl} arrival time at the l^{th} port of call on route r.

$\varphi_{r_1,l_1,r_2,l_2}$ difference (hours) between two ships' arrival time at the transshipment $\langle r_1, l_1, r_2, l_2\rangle$.

η_{r_1,l_1,r_2,l_2} auxiliary variable for transferring the gap "$\pi_{r_1 l_1} - \pi_{r_2 l_2}$" to above variable $\varphi_{r_1,l_1,r_2,l_2}$.

4.2 Decision model for regulator M_G

The regulator is the decision makers for designing the ECA, which includes the ECA width (i.e., the distance between coastline and ECA boundary) and the sulfur limit (i.e., the maximum sulfur content in marine fuel used in the ECA). The following model M_G is formulated for a regulator. The above two decision variables are denoted by w and x for the ECA width and the sulfur limit, respectively. The objective of the model M_G is to minimize the total sulfur emission of the transportation activities via both the sea and the land, which obeys the target of the regulator i.e., reducing the emission of the whole society. The model M_G is formulated as follows.

$$[\boldsymbol{M_G}]\ Minimize \sum_{r\in R} n_r \sum_{l\in L_r}\sum_{p\in P_{rl}} \lambda^*_{rlp}\left[\underbrace{s^E(x)a\left(v^{E*}_{rlp}\right)^b\left(2\sqrt{w^2+m^2_{rlp}}\right)}_{emission\ via\ sea\ (inside\ ECA)}+\underbrace{s^N a\left(v^{N*}_{rlp}\right)^b\left(d^S_{rl}-2m_{rlp}\right)}_{emission\ via\ sea\ (outside\ ECA)}\right]+\underbrace{\sum_{(i,j)\in Y} s^D u^L_{ij}\alpha^{L*}_{ij}}_{emission\ via\ land} \quad (4\text{-}1)$$

subject to: $\lambda^*_{rlp}, v^{E*}_{rlp}, v^{N*}_{rlp}, \alpha^{L*}_{ij} \in \underset{\lambda_{rlp}, v^E_{rlp}, v^N_{rlp}, \alpha^L_{ij}}{\operatorname{argmax}} Z$ (4-2)

$x \in X$ (4-3)

$w \geq 0.$ (4-4)

The objective of the above model M_G mainly contains two parts; the emission via sea and emission via land; the former one is further divided into two parts, i.e., the emissions inside ECA and outside ECA; all the above should be minimized by setting optimal values for the variable on the sulfur limit x, which is a discrete variable and belongs to the set X, and the variable on the ECA width w, which is a non-negative continuous variable. In the above model M_G, the notations λ^*_{rlp}, v^{E*}_{rlp}, v^{N*}_{rlp}, and ${\alpha^L_{ij}}^*$ are parameters, which are the solution of another decision model M_L. Different from the model M_G, the decision maker of the model M_L is the shipping liner. The model M_L is a maximization problem and its objective is denoted by Z. The values of the M_L's solved decision variables are denoted by λ^*_{rlp}, v^{E*}_{rlp}, v^{N*}_{rlp}, and ${\alpha^L_{ij}}^*$, which are used as known parameters in the regulator's model M_G. From the above, we can see that the core of the model M_G lies in the efficient solving of the model M_L, which is elaborated in the next subsection.

4.3 Decision model for shipping liner M_L

As aforementioned, this subsection proposes a model M_L for maximizing profit at a shipping liner's side. The decision variables on the ECA width w and sulfur content limits x are the input parameters for the following model M_L. Given the values of w and x, the model M_L helps liner make some operational-level decisions such as the sailing paths, speeds, and cargo allocation in the liner's shipping network.

$$[\boldsymbol{M_L}] \quad Maximize \quad Z = \underbrace{\sum_{(i,j)\in Y} c^S_{ij}\alpha^S_{ij}}_{revenue} - \underbrace{\sum_{(i,j)\in Y}\sum_{\langle r_1,l_1,r_2,l_2\rangle\in U} k^H_{r_1,l_1,r_2,l_2,i,j} c^H_{r_1,l_1,r_2,l_2}\alpha^S_{ij}}_{transshipment\ cost} -$$

$$\underbrace{\sum_{r\in R} y_r \sum_{l\in L_r}\sum_{p\in P_{rl}} \lambda_{rlp}\left[f^E(x)a\left(v^E_{rlp}\right)^b\left(2\sqrt{w^2+m^2_{rlp}}\right) + f^N a\left(v^N_{rlp}\right)^b\left(d^S_{rl}-2m_{rlp}\right)\right]}_{fuel\ cost} \tag{4-5}$$

subject to:

$$\sum_{p\in P_{rl}} \lambda_{rlp} = 1 \qquad \forall r \in R, l \in L_r \tag{4-6}$$

$$\sum_{p\in P_{rl}} \left(\frac{2\sqrt{w^2+{m_{rlp}}^2}}{v^E_{rlp}} + \frac{d^S_{rl}-2m_{rlp}}{v^N_{rlp}}\right)\lambda_{rlp} = \tau_{rl} \qquad \forall r \in R, l \in L_r \tag{4-7}$$

$$\theta^S_{ij} = \sum_{r\in R}\sum_{l\in L_r} k^S_{rlij}\tau_{rl} + \sum_{r\in R}\sum_{l\in L_r} k^S_{rlij} e_{rl} + \sum_{\langle r1,l1,r2,l2\rangle\in U} k^H_{r_1,l_1,r_2,l_2,i,j}\varphi_{r_1,l_1,r_2,l_2} \qquad \forall (i,j) \in Y \tag{4-8}$$

$$\pi_{r,l+1} = \pi_{rl} + e_{rl} + \tau_{rl} \qquad \forall r \in R, l \in L_r \qquad (4\text{-}9)$$

$$\pi_{r,|L_r|+1} = \pi_{r1} + y_r 24g \qquad \forall r \in R \qquad (4\text{-}10)$$

$$\pi_{r1} \in \{0, \cdots, (24g-1)\} \qquad \forall r \in R \qquad (4\text{-}11)$$

$$\pi_{r_2 l_2} - \pi_{r_1 l_1} + \eta_{r_1,l_1,r_2,l_2} 24g = \varphi_{r_1,l_1,r_2,l_2} \qquad \forall \langle r_1, l_1, r_2, l_2 \rangle \in U \qquad (4\text{-}12)$$

$$-y_{r_2} \leq \eta_{r_1,l_1,r_2,l_2} \leq y_{r_1} \qquad \forall \langle r_1, l_1, r_2, l_2 \rangle \in U \qquad (4\text{-}13)$$

$$\frac{\alpha_{ij}^L}{\alpha_{ij}^S} = \frac{\theta_{ij}^S}{t_{ij}^L} \qquad \forall (i,j) \in Y \qquad (4\text{-}14)$$

$$\alpha_{ij}^L + \alpha_{ij}^S = q_{ij} \qquad \forall (i,j) \in Y \qquad (4\text{-}15)$$

$$\lambda_{rlp} \in \{0,1\} \qquad \forall r \in R, l \in L_r, p \in P_{rl} \qquad (4\text{-}16)$$

$$0 < v_{rlp}^E, v_{rlp}^N \leq \overline{v} \qquad \forall r \in R, l \in L_r, p \in P_{rl} \qquad (4\text{-}17)$$

$$\tau_{rl}, \pi_{rl} \in \mathbb{Z}_+ \qquad \forall r \in R, l \in L_r \qquad (4\text{-}18)$$

$$\theta_{ij}^S \in \mathbb{Z}_+ \qquad \forall (i,j) \in Y \qquad (4\text{-}19)$$

$$\alpha_{ij}^S, \alpha_{ij}^L \geq 0 \qquad \forall (i,j) \in Y \qquad (4\text{-}20)$$

$$\eta_{r_1,l_1,r_2,l_2} \in \mathbb{Z};\ \varphi_{r_1,l_1,r_2,l_2} \in \{0, \cdots, (24g-1)\} \qquad \forall \langle r_1, l_1, r_2, l_2 \rangle \in U\,. \qquad (4\text{-}21)$$

For better understanding the above model, Figure 4 is demonstrated to explain the details (e.g., geometrical constructions) in the objective function and constraints of the model.

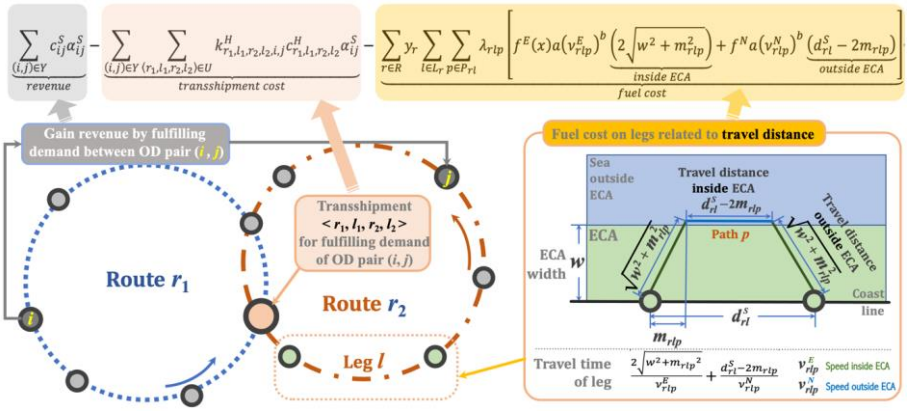

Figure 4: Illustration for the shipping liner's decision model

As shown in Figure 4, Objective Function (4-5) of the model M_L maximizes the liner's profit, which equals the revenue earned by transporting $\sum_{(i,j)\in Y} \alpha_{ij}^S$ TEU containers through its operated shipping network minus the fuel cost (i.e., majority of a liner's operation cost) and transshipment cost (i.e., the fee paid by a liner to transshipment ports). Constraints (4-6) ensure that only one path is chosen for each leg on routes. As shown in right bottom part of Figure 4, Constraints (4-7) calculate each leg's sailing

time on routes. Constraints (4-8) calculate the delivery time of fulfilling transportation demand of OD pair (i, j), including the sailing time, dwell duration at ports, and the transshipment handling time. Constraints (4-9) guarantee the arrival time continuity between two adjacent ports of call on each route. Constraints (4-10) ensure that the number of ships deployed on each route can provide a periodic service frequency, which is g days per period in this problem. Constraints (4-11) ensure that the ship deployed on route r visits the first port within the first period (i.e., g days) of the planning horizon. Constraints (4-12) and (4-13) state the arrival time difference between two ports of call at a transshipment port. Constraints (4-14) and (4-15) split the cargo volume for each OD pair into two streams; one is via sea and the other is via land. Constraints (4-16)—(4-21) define the ranges of decision variables.

In the model M_L, Objective (4-5) is nonlinear due to the bth power of variables v_{rlp}^E or v_{rlp}^N, which further times another variable λ_{rlp}; Constraints (4-7) contain nonlinear parts that are variable λ_{rlp} divided by variables v_{rlp}^E or v_{rlp}^N. The details for linearizing Objective (4-5) and Constraints (4-7) are elaborated in Appendix A. Constraints (4-14) also contain a nonlinear part that is product of two integer variables α_{ij}^S and θ_{ij}^S. The details for linearizing Constraints (4-14) are elaborated in Appendix B.

The above linearization for the model M_L is based on piecewise-linear approximation. Thus the linearized model is actually an approximation model for the original model M_L; and the approximation error could be controlled within a tolerance value ϵ. The linearized model, denoted by $\widetilde{M}_L$, is summarized as follows. The details on the above mentioned tolerance value and some of its newly added constraints as well as variables are elaborated in Appendix A.

$$[\widetilde{\boldsymbol{M}}_{\boldsymbol{L}}] \quad Maximize \quad Z = \sum_{(i,j)\in Y} c_{ij}^S \alpha_{ij}^S - \sum_{(i,j)\in Y} \sum_{\langle r_1,l_1,r_2,l_2\rangle\in U} k_{r_1,l_1,r_2,l_2,i,j}^H c_{r_1,l_1,r_2,l_2}^H \alpha_{ij}^S$$
$$- \sum_{r\in R} y_r \sum_{l\in L_r} \{\sum_{p\in P_{rl}} [f^E(x)\rho_{rlp} + f^N \mu_{rlp}]\} \quad (4\text{-}22)$$

subject to: Constraints (4-6), (4-8)–(4-13), (4-15)–(4-21), (A4)–(A5), (A15)–(A17), and (B8)–(B11).

Remark 1: By relaxing some of the integer variables in the above model as continuous variables, the obtained linear programming relaxation model (denoted by $\widetilde{M}_L^{LR}$) provides a lower bound for the original model M_L.

The lower bound could be used as a metric to evaluate the quality of the model M_L's solution solved by an algorithm in some large-scale instances.

5. Algorithms for solving models

For the proposed two models, the first key issue is to solve model M_L. Although the model can be linearized according to the methods elaborated in the appendix, the CPLEX optimization package cannot solve the linearized model in some large-scale instances. We design a tailored hybrid algorithm

based on the variable neighborhood search (VNS) meta-heuristic to solve model M_L efficiently. To solve model M_G, we suggest a genetic algorithm-based solution method.

5.1 A hybrid algorithm for solving model M_L

For solving the model M_L with large-scale instances efficiently, a hybrid algorithm is proposed by combining the VNS meta-heuristic and a two-phase procedure. After investigating the features of the model M_L, we choose the decision variable τ_{rl} as the key variable to construct the solution space for our proposed algorithm. We adopt the VNS meta-heuristic to search the best value of τ_{rl} in the solution space. For each solution in the space, its objective is evaluated by a two-phase procedure, which could be regarded as a decoding process for the solution τ_{rl}. In other words, given the value of τ_{rl}, we solve a submodel $\ddot{M}_L^{Fuel}(r,l,p)$ in phase 1, and then solve a submodel $\ddot{M}_L^{cargo}$ in phase 2, which could derive the objective value of a solution under the value of τ_{rl}. More specifically, the first submodel is solved on the basis of a proposition, while the second submodel is solved by the CPLEX directly. Subsection 5.1.2 elaborates the above two submodels. As the usual practice of algorithm design, the initialization of solution is also very important. Subsection 5.1.1 elaborates a submodel $\ddot{M}_L^{route}$ for initializing the value of the variable τ_{rl}. Subsection 5.1.3 introduces the VNS meta-heuristic for the solution improvement of τ_{rl}. In all, our proposed algorithm combines the well-known VNS meta-heuristic and a two-phase procedure, which further contains three different submodels and a proposition; thus this tailored algorithm is called as a hybrid algorithm in this study.

5.1.1 Initialization of τ_{rl}

The sailing time τ_{rl} is the first decision variable that should be determined in this hybird algorithm because it affects the path-dependent fuel cost in voyage, which further influences the cargo flows in the shipping network. Here we formulate a model $\ddot{M}_L^{route}$ to solve the sailing time τ_{rl}. In this phase of solving the model, some other decision variables such as the arrival time π_{rl}, transshipment related variables η_{r_1,l_1,r_2,l_2} and $\varphi_{r_1,l_1,r_2,l_2}$, and delivery duration via sea θ_{ij}^S are also decided.

$$\left[\ddot{M}_L^{route}\right] \quad \min \sum_{r\in R}\sum_{l\in L_r}\tau_{rl} \tag{5-1}$$

subject to: Constraints (4-8)–(4-13); (4-18); (4-20)–(4-21)

$$\theta_{ij}^S \in \mathbb{Z}_+ \qquad \forall (i,j)\in Y. \tag{5-2}$$

5.1.2 Two-phase procedure for calculating objective value given τ_{rl}

(1) Phase 1: Optimizing sailing speed and path based on proposition

Given the sailing time τ_{rl}, it is still not easy to decide the sailing speed due to the existence of the ECA. Here we formulate a model $\ddot{M}_L^{Fuel}(r,l,p)$ to decide the sailing speed variables v_{rlp}^E and v_{rlp}^N,

which influences the fuel cost in model M_L. The model $\ddot{M}_L^{Fuel}(r,l,p)$ also aims to minimize the fuel cost denoted by $\ddot{F}_{rlp}^S$, i.e., the minimum fuel cost for a ship to sail on path $p \in P_{rl}$ of leg l of route r. In the model, the v_{rlp}^E and v_{rlp}^N are decision variables and the τ_{rl} is a parameter, whose value is input from the solution of the phase 1's model.

$$\left[\ddot{M}_L^{Fuel}(r,l,p)\right] \ \ddot{F}_{rlp}^S = \min\left[f^E(x)a\cdot\left(v_{rlp}^E\right)^b\left(2\sqrt{w^2+{m_{rlp}}^2}\right)+f^N a\cdot\left(v_{rlp}^N\right)^b\left(d_{rl}^S-2m_{rlp}\right)\right] \tag{5-3}$$

subject to: Constraints (4-17)

$$\frac{2\sqrt{w^2+{m_{rlp}}^2}}{v_{rlp}^E}+\frac{d_{rl}^S-2m_{rlp}}{v_{rlp}^N}=\tau_{rl}. \tag{5-4}$$

The above model $\ddot{M}_L^{Fuel}(r,l,p)$ needs not be solved by the CPLEX. The optimal solution for the model can be determined according to the following proposition.

Proposition 1. For model $\ddot{M}_L^{Fuel}(r,l,p)$, the optimal speed within and outside ECA, i.e., $\ddot{v}_{rlp}^{E*}$ and $\ddot{v}_{rlp}^{N*}$, are calculated as follows:

when $\tau_{rl}\in[\check{T}_{rlp},\hat{T}_{rlp})$, $\ddot{v}_{rlp}^{E*}=\dfrac{2\sqrt{w^2+m_{rlp}^2}}{\tau_{rl}-\frac{d_{rl}^S-2m_{rlp}}{\overline{v}}}$ and $\ddot{v}_{rlp}^{N*}=\overline{v}$;

when $\tau_{rl}\in[\hat{T}_{rlp},\infty)$, $\ddot{v}_{rlp}^{E*}=\dfrac{2\gamma\sqrt{w^2+m_{rlp}^2}+d_{rl}^S-2m_{rlp}}{\gamma\tau_{rl}}$ and $\ddot{v}_{rlp}^{N*}=\dfrac{2\gamma\sqrt{w^2+m_{rlp}^2}+d_{rl}^S-2m_{rlp}}{\tau_{rl}}$.

The optimal objective value of model $\ddot{M}_L^{Fuel}(r,l,p)$, i.e., $\ddot{F}_{rlp}^S$, is:

$$\ddot{F}_{rlp}^S=\begin{cases}f^E(x)a\left[\tau_{rl}-\frac{d_{rl}^S-2m_{rlp}}{\overline{v}}\right]^{-b}\left(2\sqrt{w^2+{m_{rlp}}^2}\right)^{b+1}+f^N a(\overline{v})^b\left(d_{rl}^S-2m_{rlp}\right), & \check{T}_{rlp}\le\tau_{rl}<\hat{T}_{rlp}\\ f^N a\cdot(\tau_{rl})^{-b}\cdot\left[2\gamma\sqrt{w^2+{m_{rlp}}^2}+d_{rl}^S-2m_{rlp}\right]^{b+1}, & \tau_{rl}\ge\hat{T}_{rlp}\end{cases}$$

Here, $\check{T}_{rlp}=\dfrac{2\sqrt{w^2+{m_{rlp}}^2}+d_{rl}^S-2m_{rlp}}{\overline{v}}$, $\hat{T}_{rlp}=\dfrac{2\gamma\sqrt{w^2+{m_{rlp}}^2}+d_{rl}^S-2m_{rlp}}{\overline{v}}$, and $\gamma=(f^E(x)/f^N)^{1/(b+1)}$.

Proof: See Appendix C. ■

According to the optimal sailing speeds on path p of leg l on route r obtained in Proposition 1, the sailing speed within the ECA is γ times that outside the ECA when $\tau_{rl}\in[\hat{T}_{rlp},\infty)$, and the speed outside the ECA is fixed at the maximum sailing speed $\overline{v}$ and the speed within the ECA is higher than $\frac{\overline{v}}{\gamma}$ when $[\check{T}_{rlp},\hat{T}_{rlp})$. The sailing distance within the ECA $2\sqrt{w^2+m_{rlp}^2}$ can be converted to the non-

ECA distance $2\gamma\sqrt{w^2+m_{rlp}^2}$, and thus the total converted non-ECA distance on path p of leg l on route r is $2\gamma\sqrt{w^2+m_{rlp}^2}+d_{rl}^S-2m_{rlp}$. The optimal sailing speed for the converted non-ECA distance corresponding to the distance within the ECA is denoted by $\ddot{v}_{rlp}^{E\prime *}$. We further analyze $\ddot{v}_{rlp}^{E\prime *}$ and $\ddot{v}_{rlp}^{N*}$ in Corollary 1.

Corollary 1. The relationship between the optimal sailing speed for the converted non-ECA distance corresponding to the distance within the ECA and that for the distance outside the ECA is as follows: when $\tau_{rl} \in [\check{T}_{rlp}, \hat{T}_{rlp})$, $\ddot{v}_{rlp}^{E\prime *} > \ddot{v}_{rlp}^{N*}$; when $\tau_{rl} \in [\hat{T}_{rlp}, \infty)$, $\ddot{v}_{rlp}^{E\prime *} = \ddot{v}_{rlp}^{N*}$.

For a given ECA width w, define $\hat{T}_{rl}^{\max} = \frac{2\hat{\gamma}\sqrt{w^2+m_{rl\hat{p}}{}^2+d_{rl}^S-2m_{rl\hat{p}}}}{\bar{v}}$, where $\hat{\gamma}$ is the maximum γ for all possible sulfur contents x, and $\hat{p}$ is the path with the maximum $2\hat{\gamma}\sqrt{w^2+m_{rl\hat{p}}{}^2}+d_{rl}^S-2m_{rl\hat{p}}$ among all paths for leg l of route r. When $\tau_{rl} \in \left(\hat{T}_{rl}^{\max}, \infty\right)$, the choice of sailing path is affected by the sulfur limit as summarized in Proposition 2.

Proposition 2. When $\tau_{rl} \in \left(\hat{T}_{rl}^{\max}, \infty\right)$, a larger sulfur limit within the ECA leads to the optimal sailing path p with a shorter distance that reflects the detour degree (m_{rlp}) from the perspective of the shipping liner.

Proof: See Appendix D. ■

(2) Phase 2: Determining cargo flows in network

Based on the above two phases' decisions, we solve the following model $\ddot{M}_L{}^{cargo}$ to decide the cargo flows via land and sea in the shipping network. In the model $\ddot{M}_L{}^{cargo}$, the α_{ij}^S, α_{ij}^L, and λ_{rlp} are decision variables; the θ_{ij}^S is parameter determined in the phase 1. The solved objective value of the model is also the objective value of a solution for the problem.

$$\left[\ddot{M}_L{}^{cargo}\right] \quad Maximize \;\; Z = \underbrace{\sum_{(i,j)\in Y} c_{ij}^S \alpha_{ij}^S}_{revenue} - \underbrace{\sum_{(i,j)\in Y}\sum_{\langle r_1,l_1,r_2,l_2\rangle\in U} k_{r_1,l_1,r_2,l_2,i,j}^H c_{r_1,l_1,r_2,l_2}^H \alpha_{ij}^S}_{transshipment\ cost} - \underbrace{\sum_{r\in R} y_r \sum_{l\in L_r}\left\{\sum_{p\in P_{rl}} \lambda_{rlp} \ddot{F}_{rlp}^S\right\}}_{fuel\ cost} \tag{5-5}$$

subject to: Constraints (4-14)–(4-16)

$$\alpha_{ij}^S, \alpha_{ij}^L \in \mathbb{Z}_+ \qquad \forall (i,j) \in Y. \tag{5-6}$$

5.1.3 VNS meta-heuristic for improving τ_{rl}

As aforementioned at the beginning of Section 5.1, we design a neighborhood structure in VNS meta-heuristic for solution improvement of τ_{rl}. In the previous two subsections, we obtain an initial solution

for model M_L containing the main variable τ_{rl} (in Section 5.1.1) and the corresponding objective value (in Section 5.1.2). However, the τ_{rl} is solved with the objective of minimizing the sum of sailing time in Section 5.1.1, which may not be the optimal solution for model M_L aiming to maximize the liner's profit. Hence, we propose a VNS meta-heuristic to obtain a better solution. The VNS performs on a set of given neighborhood structures $\mathbb{N}_k, k = 1, \ldots, k_{max}$. We use a maximum number of VNS iterations $iter_{max}^{VNS}$ without improvement of the best solution as stopping criteria. Moreover, we define $iter_{max}^{LS}$ as the parameter which controls the number of iterations operated in the local search (LS) phase; and we define $iter_{now}^{VNS}$ as the current iteration in the VNS. The details as well as the pseudocode of the VNS procedure is elaborated in Appendix E.

5.2 Genetic algorithm for solving model M_G

The model M_G contains two core decision variables: the ECA width $w \geq 0$ and the sulfur limit $x \in X$. As the variable x is discrete and the set X is usually quite limited, the x can be enumerated during the solution process for the model M_G. Given a value of x, the model M_G with the continuous variable w is actually a complex function with argument w. As the genetic algorithm (GA) is a widely used metaheuristic for obtaining extreme values for some complex functions, this study adopts the GA to search a good result in the solution space of the variable w. More specifically, the outer loop of the algorithm for solving the model M_G is an enumeration on the variable x; and the inner component of the algorithm embeds the GA to obtain the best result on w given a certain value of x. Due to space limitation, the routine flow on the GA for solving the problem is not elaborated here.

5.3 Algorithmic improvement based on a simplified leader-follower model

The original models M_G and M_L are too complex to derive some structural properties or equilibrium results. This subsection formulates a leader-follower model by simplifying the original problem and then derive an analytical result, which could be used for initialization in the above proposed algorithm for solving the original problem. The simplified leader-follower model focuses on ships that sail between two ports, and only considers the sea transportation. The block diagram for the simplified leader-follower model is shown in Figure 5.

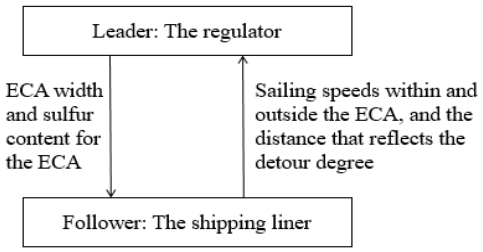

Figure 5: Block diagram of the simplified leader-follower model

The new variables are defined and the leader-follower model is formulated as follows.

Added decision variables

m_{rl}	distance that reflects the detour degree for leg l of route r under the ECA.
w_{rl}	ECA width for the ECA on leg l of route r.
v_{rl}^E	sailing speed within the ECA on leg l of route r.
v_{rl}^N	sailing speed outside the ECA on leg l of route r.
x_{rl}	sulfur content for the ECA on leg l of route r, collected in set X_{rl}.

Leader:

$$\text{Min} \quad E_{rl}^S(w_{rl}, x_{rl}) = s^E(x_{rl}) a\left(v_{rl}^E\right)^b \left(2\sqrt{{w_{rl}}^2 + {m_{rl}}^2}\right) + s^N a\left(v_{rl}^N\right)^b \left(d_{rl}^S - 2m_{rl}\right) \tag{5-7}$$

$$\text{subject to:} \quad w_{rl} \geq 0 \tag{5-8}$$

$$x_{rl} \in X_{rl}. \tag{5-9}$$

Follower:

$$\text{Min} \quad C_{rl}^S(v_{rl}^E, v_{rl}^N, m_{rl}) = f^E(x_{rl}) a\left(v_{rl}^E\right)^b \left(2\sqrt{{w_{rl}}^2 + {m_{rl}}^2}\right) + f^N a\left(v_{rl}^N\right)^b \left(d_{rl}^S - 2m_{rl}\right) \tag{5-10}$$

$$\text{subject to:} \quad \frac{2\sqrt{{w_{rl}}^2 + {m_{rl}}^2}}{v_{rl}^E} + \frac{d_{rl}^S - 2m_{rl}}{v_{rl}^N} = \bar{\tau}_{rl} \tag{5-11}$$

$$v_{rl}^E, v_{rl}^N > 0 \tag{5-12}$$

$$m_{rl} \geq 0. \tag{5-13}$$

The objective of leader problem aims to minimize the sulfur emission of ships sailing on leg l of route r via sea. The main variables in the leader model are policy-related variables w_{rl} and x_{rl}. The follower's problem is defined following the leader's action that w_{rl} and x_{rl} are determined. And the objective function is minimization of the fuel cost of ships sailing on leg l of route r via sea. v_{rl}^E, v_{rl}^N, m_{rl} are the main variables in the follower model, and $\bar{\tau}_{rl}$ is a given sailing time on leg l of route r. By analyzing this leader-follower model, we have the following property.

Proposition 3: The optimal ECA width ${w_{rl}}^*$ is 0 or $\frac{d_{rl}^S\sqrt{\gamma^2-1}}{2}$ for minimizing the sulfur emission of ships sailing on leg l of route r via sea without considering the path along the coastline within the ECA when ${w_{rl}}^* > 0$ in the leader-follower model.

Proof: See Appendix F. ■

We further consider the path along the coastline within the ECA, which will affect the design of the ECA width as summarized in Proposition 4.

Proposition 4: The optimal ECA width ${w_{rl}}^*$ is 0 or $\frac{\gamma d_{rl}^S - d_{rl}^S}{2\sqrt{\gamma^2-1}}$ for minimizing the sulfur emission of

ships sailing on leg l of route r via sea considering all sailing paths, including the path along the coastline outside the ECA when ${w_{rl}}^* = 0$ and the paths via detour points on the ECA boundary and the path along the coastline within the ECA when ${w_{rl}}^* > 0$.

Proof: See Appendix G. ■

According to Proposition 4, we further derive the relationship between the optimal sailing distances within and outside the ECA.

Corollary 2. When ${w_{rl}}^* > 0$, the optimal sailing distances within and outside the ECA are both $\frac{\gamma d_{rl}^S}{\gamma+1}$.

Proof: See Appendix H. ■

As aforementioned at the beginning of this subsection, the result of Proposition 4 can be used for the initialization in the proposed algorithm for solving the original problem; more specifically, it is applied to initializing the variable w_{rl} in the genetic algorithm for solving the model M_G. The detailed usage of the result of Proposition 4 in the algorithmic initialization is explained as follows.

The value of ${w_{rl}}^*$ obtained in Proposition 4 is oriented to one leg, i.e., leg l on route r. However, the decision variable w_{rl} in the model M_G is oriented to the whole network. Thus we should use a weighted sum of the values of ${w_{rl}}^*$ for all the legs in the network to be used as the initial value of the variable w_{rl} in the model M_G's algorithm. Then it is important to set a proper weight for each leg in the above calculation.

The objective of the leader's model is to minimize the sulfur emission. A leg l's related emission is proportional to: (i) the length of the leg, i.e., d_{rl}^S, (ii) the number of ships travelling along the leg during a certain period. The second factor is actually influenced by the number of routes that include the leg, i.e., $|\{r|l \in L_r\}|$, here $\{r|l \in L_r\}$ denotes the set of routes containing leg l. Therefore, the weight for leg l could be set as $d_{rl}^S \cdot |\{r|l \in L_r\}|$. Then the initial value of the variable w_{rl} in the model M_G's algorithm, which is denoted by $\overline{w}_{rl}$, could be calculated according to the following formula.

$$\overline{w}_{rl} = \frac{\sum_{r\in R}\sum_{l\in L_r} d_{rl}^S \cdot |\{r|l \in L_r\}| \cdot {w_{rl}}^*}{\sum_{r\in R}\sum_{l\in L_r} d_{rl}^S \cdot |\{r|l \in L_r\}|}. \quad (5\text{-}14)$$

6. Computational experiments

We conduct numerical experiments to investigate some managerial insights. The experiments contain two parts. The first part is designed to validate the efficiency of our proposed solution method and the quality of the solved solutions. After validating that our proposed methodology is effective, the second part involves applying the methodology to a series of sensitivity analyses to investigate the influence of some important parameters of the ECA design on the final performance. These computational experiments are performed on a personal computer (28 core CPUs; 2.4 GHz; 256 GB memory). The

algorithms are programmed with the technology of C# and the models embedded in the algorithms are solved by CPLEX12.5.1 (Visual Studio 2019).

6.1 Experimental setting

China has been expanding its ECA along its coastline since December 2018. The experiments in this study consider different ECA settings with respect to the ECA width and the sulfur content limit. More specifically, the ECA widths considered in the experiments range from 1 nm to 12 nm, and we consider five alternative sulfur content limits for fuel consumed within the ECA: 0.05%, 0.1%, 0.2%, 0.3%, and 0.4%. We set the largest ECA sulfur limit at 0.4% in this experiment because China has had a 0.5% global sulfur limit in force since January 1, 2020 (Zhuge et al., 2021). For the experiment, we adopt the shipping network operated by Shanghai Zhonggu Shipping Group Co. Ltd, a famous shipping company in China, which focuses on maritime shipping for domestic trade. As the ECA in China mainly influences shipping activities in China's offshore sea, it is appropriate to choose this shipping network to investigate the ECA design. In the experiments, we mainly consider ships with a capacity of more than 6,000 TEUs as these large ships have a more significant influence on emissions than feeders. For the parameters related to ship fuel consumption, we set the value of conversion factors a and b to 2×10^{-4} and 2.3, respectively, and the maximum speed to 23 knots (Zhuge et al., 2020; Wang & Meng, 2012). The dwell duration at each port of call is set within a 1–4 hour range (Qi & Song, 2012), and the transshipment cost is set in the range of 130–150 USD/TEU (Zhen et al., 2019). The average value of n_r is set to three; and the period of the shipping network, i.e., g, is set as three, which is realistic as it aligns with the timetable of services provided by the Zhonggu Shipping Group company. According to the global average bunker price from April to July in 2022 (Bunker, 2022), the price of very low sulfur fuel oil (VLSFO) used outside the ECA is set to 1,000 USD/ton (despite its name, the VLSFO results in higher sulfur emissions than MGO, which ships use inside the ECA). The volumes of cargo (in TEUs) for OD pairs are based on the container throughput of the coastal ports in the shipping network in one month, i.e., March 2022. The shipping network and the ports in experiments are shown in Figure 6.

Figure 6: The shipping network with 20 routes in the offshore sea of China

6.2 Evaluating algorithmic performance

As mentioned, we must ensure that the proposed hybrid VNS with two-phase-models algorithm is effective before using it to solve some large-scale instances to investigate the best design of the ECA in China's offshore sea. First, we conduct a series of comparative experiments to evaluate the quality of model M_L's solutions solved by our algorithm by comparing them with the optimal solution solved by the CPLEX. The comparison with the CPLEX results is designed to demonstrate the optimality gap of our proposed algorithm. Because the CPLEX needs to solve the instances within a reasonable time, the small-scale instances are used in this series of experiments. Table 1 lists the comparative results with respect to the objective value and the solution time of the two methods. According to the results shown in the column headed "Gap," it is evident that the optimality gap is relatively low, at about 4.3% on average, while the solution time of the proposed algorithm is much shorter than the time required by the CPLEX. The results imply that the proposed algorithm can solve the problem instances of model M_L efficiently.

Table 1: Evaluating optimality gap of model M_L's solutions solved by the proposed hybrid algorithm

Instances	CPLEX		Proposed hybrid algorithm		Gap (%)
ID	Z^C	T^C	Z^H	T^H	
2-6-1-1	345156	111	333406	7	3.40
2-6-1-2	348801	68	331254	6	5.03
2-6-1-3	374553	103	363448	5	2.96
2-6-1-4	383485	76	367915	6	4.06
2-6-1-5	377086	95	363663	6	3.56
2-6-1-6	354121	169	335027	7	5.39
2-6-1-7	355157	107	338566	5	4.67
2-6-1-8	371309	58	359451	8	3.19

2-6-1-9	372160	59	358033	5	3.80
2-6-1-10	360460	64	344974	9	4.30
3-8-2-1	431615	2854	416766	15	3.44
3-8-2-2	457182	2986	434609	16	4.94
3-8-2-3	488123	2938	459368	8	5.89
3-8-2-4	434182	3298	412753	14	4.93
3-8-2-5	419145	3115	395583	13	5.62
3-8-2-6	463174	3406	442641	11	4.43
3-8-2-7	463369	3263	441985	11	4.61
3-8-2-8	429192	3093	412809	16	3.82
3-8-2-9	474349	2942	449858	10	5.16
3-8-2-10	459849	3379	444166	12	3.41
Average:					4.30

Notes: (1) For example, the Instance ID "2-6-1-3" means the 3rd instance in the instance group which contains 2 routes, 6 ports, and 1 transshipment port. (2) Gap $= \frac{Z^C - Z^H}{Z^C} \times 100\%$.

Our proposed hybrid algorithm can solve the large-scale instances of model M_L, whereas the CPLEX cannot solve them in a short timeframe. The results for the large-scale experiments are listed in Table I1 of Appendix I. The results demonstrate that our algorithm can obtain much better solutions than the CPLEX using much less time than an hour.

The results in Table 1 and Table I1 validate the effectiveness of the proposed hybrid algorithm in solving the model M_L. Therefore, we use it to conduct some sensitivity analyses to investigate the best design for the ECA.

6.3 Investigating the design insights for ECAs

The design aspects of the ECA mainly relate to two decisions: the width of the ECA, which is the distance of the ECA boundary from the coastline; and the sulfur content limit for marine fuel used in the ECA. Using model M_G, we investigate these two aspects in the following two subsections.

6.3.1 Effect of the ECA boundary

The effect of ECA boundary on model M_G's objective, i.e., the total emissions produced by land and sea transportation, is investigated by changing the ECA width w while keep the maximum sulfur content x in marine fuel used in the ECA constant. In this sensitivity analysis, we test 12 instances with different ECA widths w on the basis of the shipping network shown in Figure 6. As noted earlier, the width w varies from 1 nm to 12 nm, with each step change being 1 nm. We conduct two sensitivity analyses in which the maximum sulfur content is set as $x = 0.1\%$ and then $x = 0.2\%$. The two curves are shown in Figure 7 and demonstrate similar trends. As the ECA width w increases, the objective, i.e., the total emissions produced by land and sea transportation, first grows gradually, then drops sharply, and then gradually increases. As shown in Figure 7, the sharp drops emerge when the ECA width w

equals 11 nm (10 nm) for the case with a maximum sulfur content of 0.1% (0.2%).

The reasons underlying these trends can be explained as follows. We take the case of $x = 0.1\%$ as an example. When $w \leq 10$ nm, along with the gradual increase of the ECA width w, the sailing distance in the ECA gradually increases, and a ship will reduce is sailing speed in the ECA to save on fuel consumption. However, once outside the ECA, the ship will speed up to meet the set sailing time (τ_{rl}) of a leg, which leads to an increase of sulfur emissions outside the ECA. Thus, the total sulfur emissions gradually increase. When the ECA boundary is moved further away from the coastline (e.g., when $w = 11$ nm), the ECA area becomes too large, which results in the ship sailing for what the shipping company considers to be an excessively long voyage in the ECA, and it further incurs an increase in the sailing time (τ_{rl}) required to complete the journey leg. According to Constraints (4–10), the total sailing time of a route is changed in a discrete way in a step of $24g$ hours, which also brings about discrete changes to the sailing time of some legs inside the route. More specifically, when $w \leq 10$, the sailing time of some legs remains unchanged, but when $w = 11$, a discrete change in the sailing time of some legs occurs, which makes the sailing time of some routes grow and leads to reductions of sailing speed both inside and outside the ECA; then, the sulfur emissions via sea transport decrease significantly. At the same time, the increase of the delivery time via sea implies that more goods will be transported via land than previously. Although the sulfur emission via land increases, the reduction in sulfur emissions via sea transport is greater than the increase via land transport. Therefore, the overall sulfur emissions are reduced, which is reflected in the sharp drop of the curve in Figure 7. When the ECA width continuously grows (i.e., $w \geq 11$), the trend of the curve and the reasons underlying the trend, are similar to those in the case where the ECA width $w \leq 10$. The above results indicate that a regulator should decide the ECA boundary carefully. There is an optimal value for the ECA width given a shipping network with the transportation demand of all the ODs, the configurations of the maritime ship fleets deployed on the network, and the configurations of the land transportation fleets related to these ODs. According to the Zhonggu Shipping company's shipping network and the transportation demand data, it may be appropriate to set the ECA width at about 11 nm to reduce the overall sulfur emissions for the coastal area of China. The current ECA width set by China's regulator is 12 nm, which is close to our calculated result. To further explore the effect of the ECA boundary, we extend the ECA boundary range and test some instances under six alternative values of the ECA width w (i.e., 13, 20, 30, 40, 45, and 50 nm) for the case with a maximum sulfur content of 0.1%. The results are shown in Table 2.

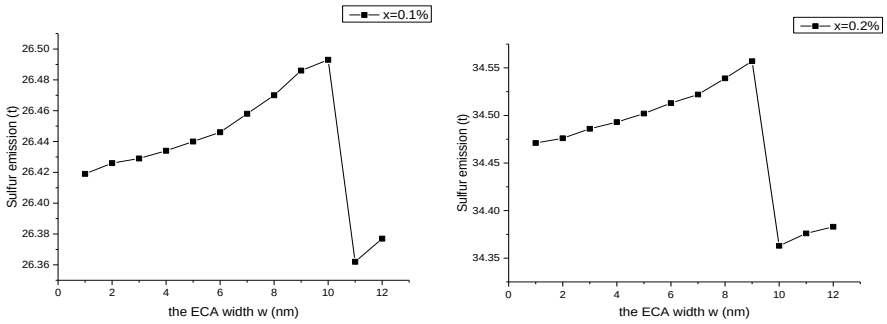

Figure 7: The overall sulfur emissions via land and sea under different ECA widths

Table 2: The overall sulfur emissions via land and sea under different ECA widths

ECA width (nm)	5	10	11	12	13	20	30	40	45	50
Sulfur emission (t)	26.44	26.49	26.36	26.38	26.40	27.56	28.42	15.51	15.02	15.02

We can obviously note that the least sulfur emission is obtained when the ECA width $w \geq 45$ nm. The reason for this result is that when the ECA boundary is moving far away from the coastline, more than 45 nm, the detour strategy (proposed in the paper) for ships becomes more and more costly. Consequently, more and more ships choose to sail inside the ECA directly for complying with the ECA policy. If the ship chooses sailing inside the ECA, the emission reduction is considerable because of the lower sulfur content of MGO consumed in the ECA. Based on these observations, it can be concluded that if the ECA width is required to be within the range of 12 nm, then the total sulfur emissions are minimized at $w = 11$ nm, and if the ECA width is allowed to exceed 12 nm, minimal sulfur emissions are achieved when $w = 45$ nm. These insights provide suggestions for China's government to design its ECA size. Specifically, this paper focuses on the effect of ECA boundary on speed and path optimization, mainly considering the case when the ECA boundary is within the range of 12 nm (i.e., $w \leq 12$nm). Thus, the optimal ECA width is set to 11 nm while keeping the maximum sulfur content 0.1% in fuel used in the ECA.

As aforementioned, the maximum sulfur content limit (i.e., the value of x) influences the optimal ECA width. More computational experiments are conducted by setting the x as five different values that ranges from 0.05% to 0.4% so as to investigate the potential influence of the maximum sulfur content limit on the optimal ECA width. Due to the limitation of space, the experimental results are shown in Appendix I(3). The results imply that when the maximum sulfur content limit becomes more and more strict (i.e., the value of x deceases), the optimal ECA width will increase or remain unchanged.

It should be noted that the factor of the ocean-bound cargoes need not be considered in our proposed

models because it is not related to the transportation demand split for OD pairs along the coastline. However, when we obtain the result of the optimal ECA width by using our proposed models, this factor should be considered for updating the above result. More specifically, suppose the optimal ECA width calculated by our models is w^*, and the total sulfur emissions via land and sea (i.e., offshore sea) is denoted by $Z_{M_G}(w^*)$, which is the lowest objective value of the model M_G. If we move the ECA boundary outward for Δ nautical miles, which means the ECA width becomes $w^* + \Delta$, the total sulfur emissions becomes $Z_{M_G}(w^* + \Delta)$, which leads to an increment emission of $Z_{M_G}(w^* + \Delta) - Z_{M_G}(w^*)$. However, for the ocean-bound cargoes, they are transported by ships that use low-sulfur fuel for Δ more nautical miles, while these ships use high-sulfur fuel for Δ less nautical miles; then the emission reduction of transporting ocean-bound cargoes, denoted by $\mathbb{F}(\Delta)$, can be calculated according to Δ and the parameters related to ships' unit emission with respect to travel distance. Then, if $\mathbb{F}(\Delta) \geq Z_{M_G}(w^* + \Delta) - Z_{M_G}(w^*)$ and $\mathbb{F}(\Delta + 1) < Z_{M_G}(w^* + \Delta + 1) - Z_{M_G}(w^*)$, the originally obtained optimal ECA width should be updated, i.e., $w^* \leftarrow w^* + \Delta$. According to the above idea, we calculate the Δ value for updating China's ECA boundary; $\Delta = 2$ nm. It means the aforementioned optimal ECA width (i.e., 11 nm) should be updated as 13 nm.

6.3.2 Effect of the sulfur limit in the ECA

As well as the ECA width, another important decision in designing the ECA is the maximum sulfur content limit x for marine fuel used in the ECA. As noted previously, we conduct a series of experiments under five alternative values of the sulfur limit x (0.05%, 0.1%, 0.2%, 0.3%, 0.4%) with a fixed value for the ECA width. The results are shown in Figure 8, where the three panels from left to right represent ECAs for $w = 9$, $w = 10$, and $w = 11$, respectively. The horizontal coordinates represent the six alternative sulfur content limits, and the longitudinal coordinates represent the total sulfur emissions. Figure 8 indicates that the optimal value for the sulfur limit inside the ECA is 0.1%. When the sulfur content limit is stricter, the price of marine fuel consumed in the ECA increases, leading ships to increase the distance that they travel outside the ECA. The high sulfur content in the fuel used outside the ECA generates a large amount of sulfur emissions, so the overall sulfur emissions increase under this ECA design. When the sulfur content limit is lowered, the sulfur content of the fuel used inside the ECA becomes higher, the price of fuel used inside the ECA becomes lower, and ships increase their sailing distances within the ECA. Thus, the sulfur emissions inside the ECA increase. The sulfur emissions outside the ECA do not change significantly, so the overall sulfur emissions gradually increase.

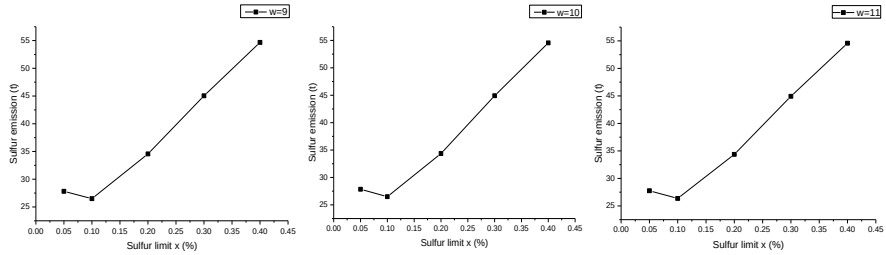

Figure 8: The overall sulfur emissions via land and sea under different sulfur limits inside the ECA

From previous analysis of the effect of ECA boundaries and sulfur limit in the ECA, we found the optimal ECA policy is that ships are permitted to sail within ECA by consuming the fuel with a maximum of 0.1% sulfur content and the ECA width is 11 nm. We further compare with the case of the current China's ECA policy that ships are required to use fuel with a sulfur content not exceeding 0.5% inside and outside ECA. Under the current ECA policy, the total sulfur emissions of sea and land transportation are 60.12 tons, which is reduced by about 56% sulfur emissions in the optimal ECA policy obtained. The results demonstrate that the optimal ECA policy in the paper can achieve sulfur emission reduction effectively and provide a reference for regulatory decision-making. Moreover, to test the effectiveness of the proposed model, we further investigate the profit earned by shipping lines (the objective of model M_L) of the case without optimization under the optimal ECA policy and compare with the results obtained by solving the model M_L under the optimal ECA policy. In the case without optimization under the optimal ECA policy, all ships sail along the shortest paths for all legs of all routes, where the profit is \$885,428. And the results of solving the model M_L under the optimal ECA policy is \$1,023,573, achieving approximately 13% of earnings increase. It can be seen that the path and speed optimization makes a significant contribution for cost reductions. To sum up, the integrated model (M_G and M_L) can be used to validate the effectiveness of the design of the ECA policy, save the operating costs of companies, and reduce sulfur emissions, which achieves a good balance relationship between the earnings and environmental impact.

6.4 Deriving managerial implications for liners

As well as deriving the above ECA design insights for the regulator, we employ the proposed liner's profit model to conduct sensitivity analysis experiments and derive some managerial implications for the practitioners in the shipping industry.

6.4.1 Effect of the fuel price

The fuels used inside and outside the ECA are usually MGO and VLSFO, respectively. Their prices, and especially the difference between them, have a great impact on the liner's fuel costs. First, we

investigate the impacts of fuel prices on the liner's profit by analyzing the first instance with 20 routes in Table I1, i.e., case 20-18-14-1. In the baseline scenario, the prices for MGO and VLSFO are 1,180 USD/ton and 1,000 USD/ton, respectively. We conduct two series of sensitivity analyses on the fuel price: (i) we set a fixed VLSFO price of 1,000 USD/ton, and vary the MGO price over eight values, i.e., 1,020, 1,060, 1,100, 1,140, 1,180, 1,220, 1,260, and 1,300 USD/ton; and (ii) we fix the MGO price at 1,180 USD/ton, and vary the VLSFO price across eight values, i.e., 840, 880, 920, 960, 1,000, 1,040, 1,080, and 1,120 USD/ton. The results of the analyses are shown in Figure 9, which indicates that the liner's profit will decrease as the MGO price increases, or as the VLSFO price changes. The reason may be that regardless of which fuel is used inside or outside the ECA, the higher the price of fuel, the larger the total fuel cost, which will reduce the liner's profit. Along the horizontal axis of Figure 9(a) (Figure 9(b)), the price difference between the two types of fuel used inside and outside ECA increases (decreases). The two curves show that the price difference between the two types of fuel has no relationship with the liner's profit. It has been proved that the price difference has an impact on voyage detours (Zhen et al., 2020; Li et al., 2020; Wang et al., 2021). However, the results in Figure 9 imply that the influence of the fuel price difference on the liner's profit (through voyage detours) is much less than its influence on the fuel cost. Finally, if we compare the approximate decreasing slopes of the curves in Figures 8(a) and 8(b), it is evident that the influence of the MGO price on the liner's profit is more significant than that of the VLSFO price. This implies that the liner may need to pay more attention to the MGO price fluctuations during its operations management than to VLSFO price fluctuations.

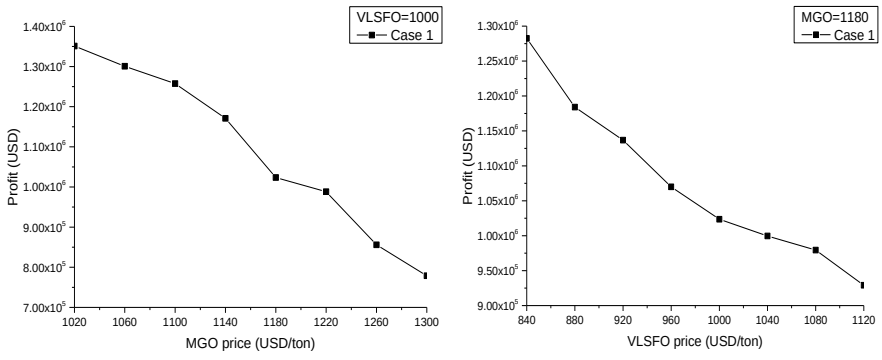

(a) (b)

Figure 9: Impact of fuel prices (MGO and VLSFO) on the liner's profit

More experiments are also conducted to investigate the influence of fuel prices on the total sulfur emission. The detailed experimental results are illustrated in Appendix I(5). The results reveal that the smaller the gap between the MGO's price and VLSFO's price, the lower is the total emission. The

reason may lie in that when the difference between the two types of the fuels is not significant, ships tend to travel for longer distance inside the ECA; then the total emission is reduced.

6.4.2 Effect of the ship deployment, dwell time, and land transportation

In addition to the fuel price, other parameters may influence the liner's profit, such as n_r (i.e., the number of ships deployed on route r), e_{rl} (i.e., ship's dwell duration at the l^{th} port of call on route r), and t_{ij}^{L} (i.e., the delivery duration for OD pair (i,j) via land) in the liner model M_L. We conduct three series of sensitivity analyses on these parameters, with the results shown in Figure 10.

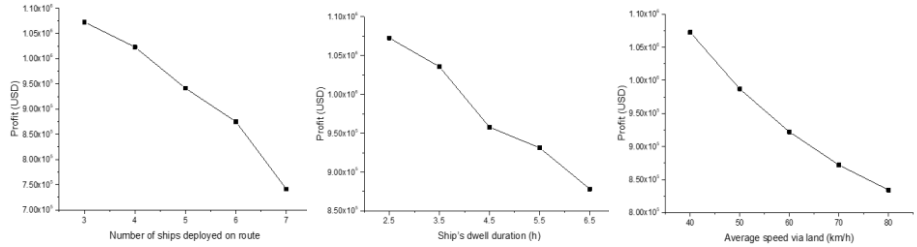

(a) (b) (c)

Figure 10: Impact of ship deployment, dwell time, and land transportation on the liner's profit

In the first series of experiments, the horizontal axis in Figure 10(a) denotes the average number of ships deployed on routes, i.e., $Avg_{\forall r} n_r$. The results show that the more ships are deployed on the routes, the less profit is earned by the liner. The reason is that more ships deployed on a route means lower sailing speeds, which reduces the demand for sea transportation relative to land transportation, and thus reduces the revenue earned by the liner. Although the low speed of ships may reduce their fuel cost, this cost reduction effect is much less than the revenue reduction effect and thus the final profit decreases.

In the second series of experiments, the horizontal axis in Figure 10(b) denotes the average duration for ships' dwelling at ports, i.e., $Avg_{\forall r,l} e_{rl}$. The results demonstrate a decreasing trend in profit as the ships' dwell duration grows. The reason is that as the duration of a ship's dwelling time at ports on a route increases, the ship's total sailing time left to complete the route decreases, and the ship needs travel at a higher speed than when dwelling time is shorter. This leads to an increase in fuel cost and thus the final profit decreases.

The third series of experiments reflect the influence of the sea transportation sector's competitor, i.e., land transportation, on the liner's profit. The horizontal axis in Figure 10(c) denotes the average speed of trucks, which is used to calculate the delivery duration for each OD pair (i,j) via land, i.e., t_{ij}^{L}. Along the horizontal axis in Figure 10(c), as the truck speed increases, the delivery duration via land (i.e., t_{ij}^{L}) becomes shorter, which leads to lower revenue or higher cost for the shipping liner in general, and thus

lower final profit is earned by the liner. The result of Figure 10(c) is also analyzed rigorously; and the result is presented in the following proposition.

Proposition 5. The liner's profit decreases in general with the increase in the average speed of trucks.

Proof: See Appendix J. ■

7. Extension of considering multiple liners' routes under varying contexts

In above proposed methodology, the liner model M_L considers one shipping liner; and the demand of OD pairs and the shipping routes are unchanging in the planning horizon. This section extends the original model M_L to consider multiple liners' routes under varying contexts, which include the seasonality of varying cargo volume of OD pairs and liners' varying routes. Before elaborating the extended model, it should be noted that the competition and/or cooperation among the multiple liners are not considered here. In this extension, the liners' model mainly consider that different liners have different shipping networks as well as different sets of routes, ships, time tables of services and etc. Their pricing decisions for price competition and/or capacity sharing for cooperation among the liners are not considered. Before elaborating the model, some sets, parameters, and variables need be redefined as follows.

Added sets of indices

N set of liners, indexed by n.

Ω set of contexts (scenarios), indexed by ω; the probability of scenario ω is denoted by $\wp(\omega)$.

Redefined sets of indices

$R_{n\omega}$ set of routes operated by liner n in scenario ω, indexed by r; $R = \bigcup_{n\in N,\omega\in\Omega} R_{n\omega}$.

$U_{n\omega}$ set of liner n's transshipment quadruples $\langle r_1, l_1, r_2, l_2\rangle$ in scenario ω; $U = \bigcup_{n\in N,\omega\in\Omega} U_{n\omega}$.

The above redefinition of sets is to extend the set of routes as well as transshipments from two dimensions (i.e., liners and scenarios). It implies that one "physical" route operated independently by two liners and is kept same in two scenarios will be regarded as four "virtual" routes in this extended model. By following this redefinition, the original model M_L needs not be modified significantly. The scenario index ω should be added into the subscripts of some parameters and variables, as follows.

Redefined parameters

$q_{ij\omega}$ total volume of cargoes transported for OD pair (i,j) via sea or land in scenario ω.

$c^S_{ij\omega}$ unit price for shipping containers for OD pair (i,j) via sea in scenario ω.

$f^E_\omega(x)$ unit cost of marine fuel with x sulfur content (USD/ton) in scenario ω.

f^N_ω unit cost of marine fuel consumed outside the ECA (USD/ton) in scenario ω.

$t_{ij\omega}^{L}$ delivery duration for OD pair (i,j) via land in scenario ω.

Redefined variables

$\alpha_{ij\omega}^{S}$ volume (TEU) of cargoes transported for OD pair (i,j) via sea in scenario ω.

$\alpha_{ij\omega}^{L}$ volume (TEU) of cargoes transported for OD pair (i,j) via land in scenario ω.

$\theta_{ij\omega}^{S}$ delivery duration for OD pair (i,j) via sea in scenario ω.

Then the objective of the original model M_L is to calculate the profit under one specific scenario ω, and is represented by $Z(\omega)$. The objective of the extended model of M_L should turn to: maximize $\sum_{\omega\in\Omega}\wp(\omega)Z(\omega)$. It should be noted that the above profit is the sum of all the liners' profit. As aforementioned, the competition and/or cooperation among the multiple liners are not considered here. Thus we do not formulate $|N|$ models for $|N|$ liners, each of which has an objective of maximizing its profit. For the interest of simplicity, we just formulate one M_L model and use the sum of their expected profits in scenarios as the objective. In addition, Constraints (4-8), (4-14) and (4-15) in the original model also need be revised as the following Constraints (7-1), (7-2) and (7-3), respectively.

$$\theta_{ij\omega}^{S} = \sum_{r\in R_{n\omega}}\sum_{l\in L_r} k_{rlij}^{S}\tau_{rl} + \sum_{r\in R_{n\omega}}\sum_{l\in L_r} k_{rlij}^{S}e_{rl} + \sum_{\langle r1,l1,r2,l2\rangle\in U_{n\omega}} k_{r_1,l_1,r_2,l_2,i,j}^{H}\varphi_{r_1,l_1,r_2,l_2} \quad \forall(i,j)\in Y, n\in N, \omega\in\Omega \qquad (7\text{-}1)$$

$$\frac{\alpha_{ij\omega}^{L}}{\alpha_{ij\omega}^{S}} = \frac{\theta_{ij\omega}^{S}}{t_{ij\omega}^{L}} \quad \forall(i,j)\in Y, \omega\in\Omega \qquad (7\text{-}2)$$

$$\alpha_{ij\omega}^{L} + \alpha_{ij\omega}^{S} = q_{ij\omega} \quad \forall(i,j)\in Y, \omega\in\Omega \qquad (7\text{-}3)$$

Due to the limitation of space, the linearization of the above model is omitted here; it is similar to that of the original model (See Appendix A and B). The algorithm for the above model is also similar to that for the original model. For the upper-level decision, the government model M_G is kept the same in this extension.

By using the extended methodology, computational experiments are conducted to calculate the ECA's optimal width w under the context with two shipping liners (Zhongggu, COSCO) and twelve scenarios (three years times four seasons). These two shipping liners are the representative liners for the cargo shipping along China's coastline. The shipping routes of the three liners and the cargo transportation demand for OD pairs may vary in different scenarios. Based on the extended context with multiple liners and scenarios, the overall sulfur emissions via land and sea under different ECA widths are shown in Figure 11. We can see that the result is similar as the previous experiment that just considers one liner and does not consider the routes' varying in seasons. The reason may lie in that the routes of liners are not obviously different from each other, and they also do not vary in seasons significantly. In addition, the Zhonggu company, which is adopted in the original experiments, is the most representative shipping

company for China's offshore sea. Thus the result in Figure 11 is similar to that in Figure 7. Results for other experiments in Section 6 are also not changed significantly, and thus are not shown here.

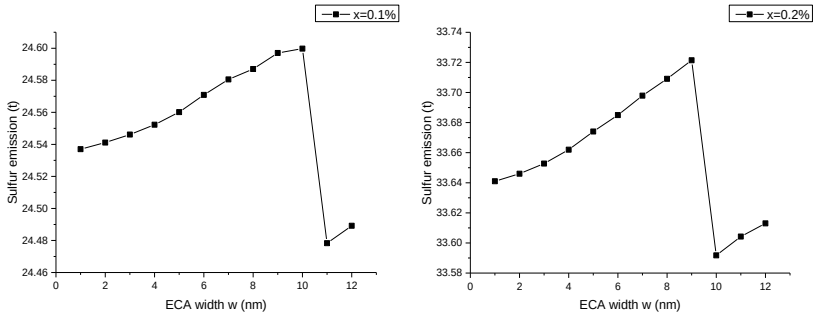

Figure 11: The sulfur emissions via land and sea considering multiple liners and multiple scenarios

We also conduct experiments to investigate the influence of the transportation demand change on the optimal ECA width. Several series of sensitivity analyses are conducted. The detailed results are illustrated in Appendix I (4). The results reveal that the transportation demand changing seems not affect the optimal ECA width.

8. Extension to heterogeneous ECA design

Although the current ECA in the offshore sea of China is homogeneous with respect to the sulfur content limit, this section conducts an explorative extension of a heterogeneous setting of the sulfur limits in the ECA. From the theoretical perspective, the heterogeneous ECA design problem dominates the homogeneous ECA design problem; in other words, the optimal solution for the heterogeneous problem should be no worse than the solution for the homogeneous one. This section elaborates the extensions of the mathematical models as well as the experimental results for the heterogeneous ECA design problem, which may be potentially useful for decision-makers when designing ECAs in the future.

8.1 ECA design with heterogeneous sulfur limits

To implement an ECA with heterogeneous sulfur limits, the offshore sea should be partitioned into several segments with different values for sulfur content limits, as demonstrated by Figure 12. The remainder of this section elaborates on the extension of our proposed mathematical models to an ECA design with a heterogeneous setting on the sulfur limit.

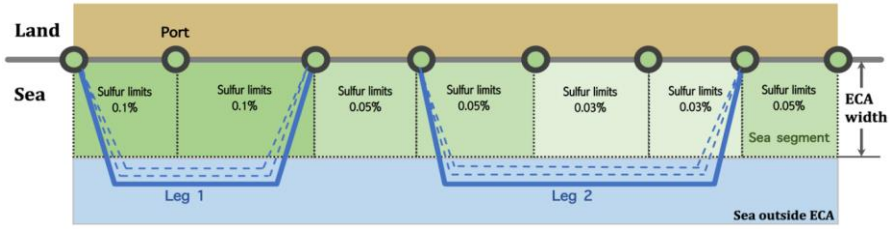

Figure 12: ECA design with a heterogeneous setting on the sulfur limit

In contrast to the homogeneous ECA design problem, in the heterogeneous problem, one leg may cross multiple sea segments with different sulfur limits. For the example in Figure 12, the sailing paths of Leg 1 inside the ECA should obey an identical sulfur limit, i.e., 0.1%. However, Leg 2 crosses sea segments with two different sulfur limits, i.e., 0.05%, and 0.03%. In this case, when determining the unit sulfur emissions $s^E(x)$ and unit fuel cost $f^E(x)$, we should consider both $s^E(0.05\%)$ and $s^E(0.03\%)$, and both $f^E(0.05\%)$ and $f^E(0.03\%)$. Here, the extended model adopts an approximation approach to handle this issue; that is, we use the average values, i.e., $[s^E(0.05\%) + s^E(0.03\%)]/2$ and $[f^E(0.05\%) + f^E(0.03\%)]/2$ to reflect the unit sulfur emissions and unit fuel cost for Leg 2, respectively. More specifically, for each leg l on route r, we define the index of two related sea segments as h^1_{rl} and h^2_{rl}. The new decision variable x_h, i.e., the sulfur content limit for sea segment h, is defined to replace the original decision variable x. Then, the unit sulfur emission $s^E(x)$ and unit fuel cost $f^E(x)$ in the previous models' objectives are replaced by the average values $\left[s^E\left(x_{h^1_{rl}}\right) + s^E\left(x_{h^2_{rl}}\right)\right]/2$ and $\left[f^E\left(x_{h^1_{rl}}\right) + f^E\left(x_{h^2_{rl}}\right)\right]/2$, respectively.

The models for the regulator and the shipping liners to optimize the ECA design under the heterogeneous sulfur limits are extended in Sections 8.2 and 8.3, respectively.

8.2 Revised model M'_G for regulator

Before formulating the two models for the regulator and the shipping liners in the context of the heterogeneous ECA, the notations for the parameters and decision variables are listed as follows.

Added sets of indices

H	set of sea segments, indexed by h.
h^1_{rl}, h^2_{rl}	index of two sea segments related to leg l on route r.

Added decision variables

x_h	sulfur content limit for sea segment h in the ECA design.

For the regulator, i.e., the decision-maker designing the ECA, the core decision is the sulfur limits in

each sea segment, i.e., x_h. The following model M_G' is formulated for the regulator, which is similar to the previously proposed model M_G. The main difference between the two models lies in the emissions inside the ECA: the $s^E(x)$ in the previous objective is replaced by an average value $\left[s^E\left(x_{h_{rl}^1}\right) + s^E\left(x_{h_{rl}^2}\right)\right]/2$ because each leg is related to two sea segments that may have different sulfur limits under the heterogeneous ECA. Model M_G' is formulated as follows.

$$[\boldsymbol{M_G'}] \quad \text{Minimize} \quad \sum_{r\in R} n_r \sum_{l\in L_r} \sum_{p\in P_{rl}} \lambda_{rlp}^* \left[\underbrace{\frac{s^E\left(x_{h_{rl}^1}\right)+s^E\left(x_{h_{rl}^2}\right)}{2} a\left(v_{rlp}^{E*}\right)^b \left(2\sqrt{w^2+m_{rlp}^2}\right)}_{emissions\ via\ sea\ (inside\ ECA)} + \underbrace{s^N a\left(v_{rlp}^{N*}\right)^b \left(d_{rl}^S - 2m_{rlp}\right)}_{emissions\ via\ sea\ (outside\ ECA)} \right] + \underbrace{\sum_{(i,j)\in Y} s^D u_{ij}^L \alpha_{ij}^{L*}}_{emissions\ via\ land} \tag{8-1}$$

subject to Constraints (4-2) and (4-4)

$$x_h \in X \qquad \forall h \in H. \tag{8-2}$$

8.3 Revised model M_L' for the shipping liner

Based on the previously proposed model M_L, model M_L' is formulated to maximize profit from the shipping liner's perspective. The decision variable x_h on the sulfur content limits in the heterogeneous ECA is linked to the variables $x_{h_{rl}^1}$ and $x_{h_{rl}^2}$, which state the sulfur content limit for the two sea segments involved in each journey leg. The values of $x_{h_{rl}^1}$ and $x_{h_{rl}^2}$ are the input parameters for the following model M_L'. Given these values, the model helps the shipping liner make operational-level decisions such as the sailing speed and cargo allocation in their shipping network.

$$[\boldsymbol{M_L'}] \quad \text{Maximize} \quad Z = \underbrace{\sum_{(i,j)\in Y} c_{ij}^S \alpha_{ij}^S}_{revenue} - \underbrace{\sum_{(i,j)\in Y} \sum_{\langle r_1,l_1,r_2,l_2\rangle\in U} k_{r_1,l_1,r_2,l_2,i,j}^H c_{r_1,l_1,r_2,l_2}^H \alpha_{ij}^S}_{transshipment\ cost} -$$

$$\underbrace{\sum_{r\in R} y_r \sum_{l\in L_r} \sum_{p\in P_{rl}} \lambda_{rlp} \left[\frac{f^E\left(x_{h_{rl}^1}\right)+f^E\left(x_{h_{rl}^2}\right)}{2} a\left(v_{rlp}^E\right)^b \left(2\sqrt{w^2+m_{rlp}^2}\right) + f^N a\left(v_{rlp}^N\right)^b \left(d_{rl}^S - 2m_{rlp}\right) \right]}_{fuel\ cost} \tag{8-3}$$

subject to Constraints (4-6) – (4-21)

Objective (8-3) of model M_L' maximizes the liner's profit. The objective as well as the constraints are similar to those of the previous model M_L. The only difference between the two models lies in the objectives, as $f^E(x)$ in the previous model's objective is replaced by $\left[f^E\left(x_{h_{rl}^1}\right) + f^E\left(x_{h_{rl}^2}\right)\right]/2$. As the extended models are similar to the previous ones, the algorithms for solving the models elaborated in Section 5 can also be applied to the above extended models. Thus, the algorithmic strategies for the

extended models are omitted here to save space.

8.4 Numerical study for a heterogeneous ECA design for China's offshore sea

We conduct experiments using the ECA in China's offshore sea as an example. For the coastline and ports shown in Figure 6, the offshore sea is partitioned into 14 sea segments. As shown in Figure 6, the five ports on the coastline from Dalian (DL) to Yantai (YT) belong to the Bohai, which is China's internal sea. Thus, we regard the coastline from DL to YT as one sea segment rather than as four segments in the experiment on the heterogeneous ECA design. Then, there are 14 sea segments considered in the following experiment. The same 20 ship routes are considered in the experiments and the same five alternatives for the limits on the sulfur content of fuel. The results of the previous experiments (see Figures 6 and 7) indicate that the threshold values for the optimal ECA width (w) setting is about 9–11 nm; we set $w = 10$ in the following experiment. By solving model M'_G, the sulfur limits in each segment of the offshore sea can be obtained.

Table 3: Results of heterogeneous setting on sulfur limits for China's offshore sea ($w = 10$)

River segments	DL-YT	YT-QD	QD-RZ	RZ-LYG	LYG-SH	SH-NB	NB-TZ	TZ-WZ	WZ-FZ	FZ-QZ	QZ-XM	XM-ST	ST-SZ	SZ-ZH
sulfur content limit	0.05%	0.1%	0.1%	0.2%	0.1%	0.05%	0.2%	0.3%	0.05%	0.05%	0.1%	0.05%	0.05%	0.3%

Table 3 illustrates the optimal setting of sulfur limits in each sea segments. The total sulfur emissions from sea and land transportation amount to 25.044 tons. However, the homogenous setting on sulfur limits is usually implemented in reality for ease of administration. If the offshore sea ECA is implemented with a homogenous setting of a 0.05% sulfur limit, the total sulfur emissions of the sea and land transportation are 27.848 tons. In a similar way, we calculate the results (i.e., the total sulfur emissions) under the alternative homogenous sulfur limits, with the results listed in Table 4.

Table 4: Comparison of homogenous and heterogeneous settings on sulfur limits ($w = 10$)

	Homogenous setting					**Heterogeneous setting**
Sulfur limits	0.05%	0.1%	0.2%	0.3%	0.4%	As shown in Table 2
Total sulfur emission (ton)	27.848	26.493	34.363	44.906	54.554	25.044

The comparative experiments validate the necessity of considering the heterogeneous setting on sulfur limits for an offshore sea ECA. The heterogeneous ECA can bring about a 5.5% emission reduction (5.5%≈(26.493−25.044)/26.493) relative to those under the homogeneous ECA with the lowest emissions standard.

To further validate the improved performance of the heterogeneous sulfur limit setting over the

homogeneous setting, we reconduct the above experiments with the ECA width set at 12 nm, which is the current policy in China. The results, shown in Tables I2 and I3 in Appendix I, demonstrate that the heterogeneous ECA can reduce emissions by an additional 4.6% compared with the homogenous setting for the case with $w = 12$. The results further validate the need to consider the heterogeneous setting on sulfur limits for the offshore sea in China even under the current ECA width. Although China's current ECA has a homogenous sulfur limit, an ECA with a heterogeneous setting on the sulfur limit is worth investigating, as it may potentially reduce total emissions further from a theoretical perspective.

9. Conclusions

This paper conducts an explorative study of ECA designs based on mathematical programming. We propose an EC design model for regulatory decision-makers that aims to minimize the total sulfur emissions via different transportation methods. Embedded in this model, we propose a liner's model designed to maximize the liner's profit; solving this model provides the values of the parameters in the regulatory decision-maker's model. We suggest algorithms to solve these models efficiently. By applying the proposed models and the suggested algorithms in the design of the ECA for China's offshore sea, we obtain some potentially useful implications for the regulator as well as the shipping liners from numerical experiments based on real data. We further investigate a cutting-edge extension of the ECA design to further improve the effectiveness of emissions abatement. By comparing our results with the relevant literature, we identify the main contributions of this study from the following three perspectives.

From the methodological perspective, to the best of our knowledge, this paper is the first to propose a mixed-integer programming model-based methodology for ECA design optimization. For this strategically important environmental policy design, few studies adopt mathematical modeling-based methods. The mathematical programming adopted in this study is used to formulate an optimization model with the aim of minimizing social total sulfur emissions by determining the boundary and sulfur limit of an ECA. In the regulator's decision model, we embed a liner model with the aim of maximizing liner profit. The nested models are built on a network of the major ports (cities) along the coastline. Given the transportation demand among these ports, the nested models determine the ECA design and the liner's decisions to minimize the total emissions from both sea and land transportation activities. In terms of both the adopted modeling method and the factors considered, this study is significantly different from those in the literature.

From the perspective of a novel ECA design, this paper proposes a cutting-edge concept for the ECA design, i.e., the heterogeneous ECA with respect to the sulfur limit. Currently, ECAs around the world

tend to be homogeneous, as the homogenous design is easy to implement in practice. However, from a theoretical perspective, the heterogeneous ECA design is preferrable to the homogeneous one because it reduces emissions further. Therefore, we extend the above nested models to the context of the heterogeneous ECA. We conduct numerical experiments to validate the extension and demonstrate the benefit of considering the heterogeneous ECA through a case study of the ECA design for China's offshore sea. This cutting-edge concept for ECA design and the proposed methodology for this concept could provide a useful and novel reference for regulatory decision-making on ECAs.

From the perspective of managerial insights, we conduct numerical experiments in the context of China's offshore sea ECA. The results indicate that the solved optimal ECA boundary is about 11 nm from the coastline, which is slightly less than the 12 nm between the current ECA boundary and the coastline. For the sulfur limit, the solved optimal value is 0.1%, which is stricter than the current 0.5% sulfur limit under China's ECA policy. The experimental results validate the necessity of the heterogeneous ECA design, demonstrating that it could reduce emissions by a further 5% compared with the lowest emissions requirements under the homogeneous ECA. As well as the insights provided for the regulator noted above, we obtain some insights for shipping liners. For example, we determine that the liner's profit will decrease when the MGO and VLSFO prices increase and that the impact of the price of the former price is more significant than the price of the latter. In addition, the number of ships deployed on routes, the length of port dwell times, and trucks' speed in land transportation also influence the liner's profit.

This study is subject to some limitations. For example, the algorithms designed in this study are heuristic rather than an exact solution method. To obtain more precise results, we could attempt to develop exact solution methods to solve these models in the future. In regard to model formulation, the transportation demand split for each OD pair is based only on the delivery time, and future studies could consider additional metrics related to this aspect. In addition, as indicated by Zisi et al. (2021), the global sulfur cap will increase CO_2 emissions (Wang et al., 2020); how to optimize ECAs and related policies to reduce both sulfur and greenhouse gas emissions is another interesting and challenging research topic for the future. Finally, the cost of scrubber may affect the detour behavior. If the cost is below a certain threshold, some ships may be retrofitted with the scrubbers; then these ships can travel inside the ECA along the shortest path of some legs. The threshold value may depend on the ECA width, the lengths of these legs, the gap between MGO's price and VLSFO's price, amongst others. Future researches could be conducted to investigate a number of cases with different possible threshold values (or ranges) for the scrubber cost. Then some new insights for ECA design could be obtained by considering the above factor.

Acknowledgements

Thanks are due to the Editor-in-Chief, the Area Editor, the Associate Editor and the referees for their valuable comments that helped improve the quality of this paper significantly.

Commented [HNP1]:

Commented [HNP2R1]: I think it is better to omit the names of the Editors, AEs etc.

References

Agarwal, R. & Ergun, Ö. (2010) Network design and allocation mechanisms for carrier alliances in liner shipping. *Operations Research* 58(6): 1726–1742.

Browning, L., Hartley, S., Bandermehr, A., Gathright, K. & Miler, W. (2012) Demonstration of fuel switching on oceangoing vessels in the Gulf of Mexico. *Journal of the Air & Waste Management Association* 62(9): 1093–1101.

Cariou, P., Cheaitou, A., Larbi, R. & Hamdan, S. (2018) Liner shipping network design with emission control areas: A genetic algorithm-based approach. *Transportation Research Part D: Transport and Environment* 63: 604–621.

Chang, Y.T., Roh, Y. & Park, H. (2014) Assessing noxious gases of vessel operations in a potential emission control area. *Transportation Research Part D: Transport and Environment* 28: 91–97.

Chen, L., Yip, T.L. & Mon, J. (2018) Provision of emission control area and the impact on shipping route choice and ship emissions. *Transportation Research Part D: Transport and Environment* 58: 280–291.

Choi, B.C., Lee, K., Leung, J.Y.T., Pinedo, M.L. & Briskorn, D. (2012) Container scheduling: Complexity and algorithms. *Production and Operations Management* 21(1): 115–128.

Chou, C.C., Kuo, F.T., Gou, R.H. Tsai, C.L., Wong, C.P. & Tsou, M.C. (2010) Application of a combined fuzzy multiple criteria decision making and optimization programming model to the container transportation demand split. *Applied Soft Computing* 10(4): 1080–1086.

Dai, L., Hu, H., Wang, Z., Shi, Y. & Ding, W. (2019) An environmental and techno-economic analysis of shore side electricity. *Transportation Research Part D: Transport and Environment* 75: 223–35.

De, A., Mamanduru, V.K.R., Gunasekaran, A., Subramanian, N. & Tiwari, M.K. (2016) Composite particle algorithm for sustainable integrated dynamic ship routing and scheduling optimization. *Computers & Industrial Engineering* 96: 201–215.

Doudnikoff, M. & Lacoste, R. (2014) Effect of a speed reduction of containerships in response to higher energy costs in sulphur emission control areas. *Transportation Research Part D: Transport and Environment* 28: 51–61.

Eberhart, R. & Kennedy, J. (1995) A new optimizer using particle swarm theory. In: *Proceedings of the1995 IEEE International Conference on Neural Network*: 1942–1948.

Fagerholt, K., Gausel, N.T., Rakke, J.G. & Psaraftis, H.N. (2015) Maritime routing and speed optimization with emission control areas. *Transportation Research Part C: Emerging Technologies* 52: 57–73.

Fagerholt, K. & Psaraftis, H.N. (2015) On two speed optimization problems for ships that sail in and out of emission control areas. *Transportation Research Part D: Transport and Environment* 39: 56–64.

Fransoo, J.C. & Lee, C.Y. (2013) The critical role of ocean container transport in global supply chain performance. *Production and Operations Management* 22: 253–268.

Gu, Y. & Wallace, S.W. (2017) Scrubber: A potentially overestimated compliance method for the emission control areas: The importance of involving a ship's sailing pattern in the evaluation. *Transportation Research Part D: Transport and Environment* 55: 51–66.

Holmgren, J., Nikopoulou, Z., Ramstedt, L. & Woxenius, J. (2014) Modelling modal choice effects of regulation on low-sulphur marine fuels in Northern Europe. *Transportation Research Part D: Transport and Environment* 28: 62–73.

Lee, C.Y., Shu, S. & Xu, Z. (2021) Optimal global liner service procurement by utilizing liner service schedules. *Production and Operations Management* 30(3): 703–714.

Li, C., Qi, X. & Lee, C.Y. (2015) Disruption recovery for a vessel in liner shipping. *Transportation Science* 49(4): 900–921.

Li, L., Gao, S., Yang, W. & Xiong, X. (2020) Ship's response strategy to emission control areas: From the perspective of sailing pattern optimization and evasion strategy selection. *Transportation Research Part E: Logistics and Transportation Review* 133: 101835.

Li, L., Pan, Y., Gao, S. & Yang, W. (2022) An innovative model to design extreme emission control areas (ECAs) by considering ship's evasion strategy. *Ocean and Coastal Management* 227: 106289.

Li, Z.C. & Sheng, D. (2016) Forecasting passenger travel demand for air and high-speed rail integration service: A case study of Beijing-Guangzhou corridor, China. *Transportation Research Part A: Policy and Practice* 94: 397–410.

Lu, T., Fransoo, J.C. & Lee, C.Y. (2017) Carrier portfolio management for shipping seasonal products. *Operations Research* 65(5): 1250–1266.

Ma, D., Ma, W., Jin, S. & Ma, X. (2020) Method for simultaneously optimizing ship route and speed with emission control areas. *Ocean Engineering* 202: 107170.

Ma, W., Lu, T., Ma, D., Wang, D. & Qu, F. (2021) Ship route and speed multi-objective optimization considering weather conditions and emission control area regulations. *Maritime Policy & Management* 48(8): 1053–1068.

Meng, Q., Wang, S., Andersson, H. & Thun, K. (2014) Containership routing and scheduling in liner shipping: overview and future research directions. *Transportation Science* 48(2): 265–280.

Panagakos, G.P., Stamatopoulou, E.V. & Psaraftis, H.N. (2014) The possible designation of the Mediterranean Sea as a SECA: A case study. *Transportation Research Part D: Transport and Environment* 28: 74–90.

Psaraftis, H.N., & Kontovas, C.A. (2010) Balancing the economic and environmental performance of maritime transportation. *Transportation Research Part D: Transport and Environment* 15: 458–462.

Qi, Y., Harrod, S., Psaraftis, H.N., & Lang, M. (2022) Transport service selection and routing with carbon emissions and inventory costs consideration in the context of the Belt and Road Initiative. *Transportation Research Part E: Logistics and Transportation Review* 159: 102630.

Qi, X. & Song, D.P. (2012) Minimizing fuel emissions by optimizing vessel schedules in liner shipping with uncertain port times. *Transportation Research Part E: Logistics and Transportation Review* 48(4): 863–880.

Roy, D., de Koster, R. & Bekker, R. (2020) Modeling and design of container terminal operations. *Operations Research* 68(3): 686–715.

Sheng, D., Meng, Q. & Li, Z.C. (2019) Optimal vessel speed and fleet size for industrial shipping services under the emission control area regulation. *Transportation Research Part C: Emerging Technologies* 105: 37–53.

Ship and Bunker (2022) World bunker prices. https://shipandbunker.com/prices.

Sun, Y., Yang, L. & Zheng, J. (2020) Emission control areas: More or fewer? *Transportation Research Part D: Transport and Environment* 84: 102349.

Svindland, M. (2018) The environmental effects of emission control area regulations on short sea shipping in Northern Europe: The case of container feeder vessels. *Transportation Research Part D: Transport and Environment* 61: 423–430.

Tan, Z., Zhang, M., Shao, S., Liang, J. & Sheng, D. (2022) Evasion strategy for a coastal cargo ship with unpunctual arrival penalty under sulfur emission regulation. *Transportation Research Part E: Logistics and Transportation Review* 164: 102818.

Tierney, K., Áskelsdóttir, B., Jensen, R.M. & Pisinger, D. (2015) Solving the liner shipping fleet repositioning problem with cargo flows. *Transportation Science* 49(3): 652–674.

UNEP (United Nations Environment Programme) (2022) IMO body grants green light to the proposal on curbing emissions from ships in the Mediterranean. https://www.unep.org/unepmap/news/news/imo-body-grants-green-light-joint-proposal-curbing-

emissions-ships-mediterranean.

Vierth, I., Karlsson, R. & Mellin, A. (2015) Effects of more stringent sulphur requirements for sea transports. *Transportation Research Procedia* 8: 125–135.

Wang, T., Du, Y., Fang, D. & Li, Z.-C. (2020) Berth allocation and quay crane asssignment for the trade-off between service efficiency and operating cost considering carbon emission taxation. *Transportation Science* 54(5): 1307–1331.

Wang, S. & Meng, Q. (2012) Sailing speed optimization for container ships in a liner shipping network. *Transportation Research Part E: Logistics and Transportation Review* 48(3): 701–714.

Wang, S., Zhuge, D., Zhen, L. & Lee, C.Y. (2021) Liner shipping service planning under sulfur emission regulations. *Transportation Science* 55(2): 491–509.

Wang, Y. & Meng, Q. (2020) Semi-liner shipping service design. *Transportation Science* 54(5): 1288–1306.

Xiong, J., Qi, X., Fu, Z. & Zha, W. (2020) Split demand one-to-one pickup and delivery problems with the shortest-path transport along real-life paths. *IEEE Access* 8: 150539–150554

Zhang, Q., Zheng, Z., Wan, Z. & Zheng, S. (2020) Does emission control area policy reduce sulfur dioxides concentretion in Shanghai? *Transportation Research Part D: Transport and Environment* 81: 102289.

Zhen, L., Hu, Z., Yan, R., Zhuge, D. & Wang, S. (2020) Route and speed optimization for liner ships under emission control policies. *Transportation Research Part C: Emerging Technologies* 110: 330–345.

Zhen, L., Li, M., Hu, Z., Lv, W. & Zhao, X. (2018) The effects of emission control area regulations on cruise shipping. *Transportation Research Part D: Transport and Environment* 62: 47–63.

Zhen, L., Wang, S., Laporte, G. & Hu, Y. (2019) Integrated planning of ship deployment, service schedule and container routing. *Computers & Operations Research* 104: 304–318.

Zheng, J., Zhang, H., Yin, L., Liang, Y., Wang, B., Li, Z., Song, X. & Zhang, Y. (2019) A voyage with minimal fuel consumption for cruise ships. *Journal of Cleaner Production* 215: 144–153.

Zhuge, D., Wang, S. & Wang, D.Z.W. (2021) A joint liner ship path, speed and deployment problem under emission reduction measures. *Transportation Research Part B: Methodological* 144: 155–173.

Zhuge, D., Wang, S., Zhen, L. & Laporte, G. (2020) Schedule design for liner services under vessel speed reduction incentive programs. *Naval Research Logistics* 67(1): 45–62.

Zis, T. & Psaraftis, H.N. (2017) The implications of the new sulphur limits on the European Ro-Ro sector. *Transportation Research Part D: Transport and Environment* 52: 185–201.

Zis, T. & Psaraftis, H.N. (2019) Operational measures to mitigate and reverse the potential modal shifts due to environmental legislation. *Maritime Policy & Management* 46(1): 117–132.

Zis, T., Psaraftis, H.N., Panagakos, G. & Kronbak, J. (2019) Policy measures to avert possible modal shifts caused by sulphur regulation in the European Ro-Ro sector. *Transportation Research Part D: Transport and Environment* 70: 1–17.

Zisi, V., Psaraftis, H.N., & Zis, T. (2021) The impact of the 2020 global sulfur cap on maritime CO_2 emissions. *Maritime Business Review* 6(4): 339–357.